

## Reply to comments from Referees

We would like to thank the editor and two anonymous referees whose comments helped us improve the manuscript. Below we give a point-to-point response to address the referees' comments. The original comments are in blue italics and our responses are in black. The corrections are marked as red color in the attached revised manuscript.

### **1. Response to Anonymous Referee #1**

*The Authors have done an extremely commendable revision to this manuscript. Despite the highly limited nature of their observational dataset, they have derived insight into some of the competing HONO mechanisms in the Beijing atmosphere under haze and clear pollution conditions. Pending some minor revisions and clarifications, the paper is acceptable for publication in Atmospheric Chemistry and Physics.*

#### **Minor Comments:**

*1. The Authors state in a number of places throughout the manuscript that aerosol production of HONO under haze conditions is dominant. This is incorrect. It is significant, but in the comparison against the ground source throughout the nocturnal boundary layer, aerosol production still only accounts for one third of the total HONO produced. This estimate is made using the upper limit for NO<sub>2</sub> reactive uptake from the literature, so it is likely less significant than reported and more in line with a wealth of prior studies. The Authors need to do a better job of performing their calculations using upper and lower limits instead of just an upper limit estimate. A conservative calculation or one which includes the variability in the observations is more reliable. Specific comments below provide some areas where this improvement is required to produce a more balanced interpretation of the dataset. Given the very limited nature of the observations, such analysis is likely to provide more robust insight for comparison when more targeted measurements are made in the future, raising the impact of this work.*

**Response:** Thank you very much for your valuable comments and suggestions. We have revised the manuscript according to the referee's specific comments below. Considering the upper and lower

limits of uptake coefficient of NO<sub>2</sub> as suggested, the uptake coefficient of  $5 \times 10^{-6}$  have been taken into account in the calculation and interpretation of the dataset. The aerosol production of HONO is an important nocturnal HONO source during haze episodes. The aerosol surface dominates HONO production aloft by heterogeneous uptake of NO<sub>2</sub> during haze episodes, and the surface production of HONO and direct emissions into the overlying air are minor contributors. The statements have been revised as the referee suggested.

*2. In Section 3.2 the Authors discuss the decreasing slopes determined using orthogonal least squares analysis. First, why the orthogonal approach was used is not clear, but presumably this was used as an extension from the revised intercomparison of the HONO measurements. The error in the measurement height must be quite a lot smaller than in the HONO measurement, which means that a least-squares regression is more likely appropriate. In either case, no examples of the regression line through the data are provided, nor are the parameters used to constrain the regression line. This limits the ability of bias in these trends to be identified. Were regressions performed through HONO data only above the surface layer? There is an exponential decrease in HONO with altitude within the surface layer that would be incorrect to apply a linear trend to, where the lowest HONO observation having the highest mixing ratio would significantly affect the slope of the line. The Authors need to clarify this approach in the manuscript so it can be compared to in future studies.*

**Response:** Thanks for the comment and suggestion. As the referee suggested, we used the linear squares regression of HONO and NO<sub>2</sub> to altitude to evaluate the nocturnal gradient of HONO and NO<sub>2</sub>. Vertical profile data were used above the surface layer and 10 m vertical average from the surface to 240 m above ground level (AGL) to constrain the regression line, which has been clarified in the revised manuscript. An example of the regression line of HONO and NO<sub>2</sub> were added in the supplementary in formation as suggested. The alterations in the values of the slopes were revised throughout the manuscript.

*3. The Authors report 1-sigma limit of detection (LOD). This is a gross error and misrepresentation of instrumental capability. Detection limits are standardly reported at 3-sigma which results in measurements with approximately 50 % error, decreasing quickly to 10 % error (or less) at the 10-sigma threshold (limit of quantitation). Report the 3-sigma LOD and indicate where this threshold*

*lies for each instrument on the Figures associated with the intercomparison and also on any plots of HONO mixing ratios where measurements are below the 3-sigma LOD. The Authors need to revise their error assigned to data between the 3-sigma and 10-sigma levels to be at least +/- 20 % of the measured value, while data below the 3-sigma LOD should be reported with +/- 100 % uncertainty. Finally, while the errors of the HONO measurements from the IBBCEAS are quantified nicely, the accuracy from the intercomparison is not actually reported. Once the LOD error re-analysis has been completed, then the slopes from the resulting intercomparisons should give a good estimate of between-instrument accuracy.*

**Response:** Thanks for the comment and suggestion. As the referee suggested, the  $3\sigma$  limit of detection (LOD) of IBBCEAS instrument was reported in the manuscript. The errors assigned to data between the  $3\sigma$  and  $10\sigma$  were modified, and Figure 2 was also revised as suggested. As the referee pointed out, we re-analyzed the LOD error and reported the relative accuracy of comparison between the different instruments in the manuscript.

**Detailed Comments:**

*1. Lines 34-37: The results of this analysis need to be updated to reflect the relative importance under haze and clean conditions according to comments below.*

**Response:** We have updated and modified this analysis as the referee suggested.

*2. Lines 49-51: The references used in this sentence appear to be placed backwards. Swap them.*

**Response:** Revision has made as the referee suggested.

*3. Line 87: Should be 'Americas'*

**Response:** Revision has made as the referee suggested.

*4. Line 118: Should be '...aerosol surfaces play a...'*

**Response:** Revision has made as the referee suggested.

*5. Lines 161-162: Please provide an estimate of the total path length.*

**Response:** An estimate of the total optical path length has been added in the manuscript as suggested.

6. Lines 164-174: Revise according to Minor Comment 3. Be very clear in how the 3-sigma LOD was calculated so it can be used for comparison by others who also measure HONO by IBBCEAS. It is too bad that a standard amount of gas phase HONO was not delivered to these systems to ensure that inlet or cavity-sorption losses of HONO were not changing over time and impacting the accuracy of the measurements.

**Response:** Thanks for the comment and suggestion. We have calculated the  $3\sigma$  LOD of the IBBCEAS instrument as suggested, which has been modified in the manuscript. As the referee pointed out, a HONO standard generator was used to determine the sample loss of HONO. In the experiment, the RH was about 65% and the temperature was about 23 °C, the sample loss of HONO was found to be ~2.0% as shown in Figure 1. The variation of HONO sample loss over time was negligible. The similar approach was used to determine the sample loss of NO<sub>2</sub> and found that it was negligible. A more detailed description of the IBBCEAS instrument can be found in our published manuscript (Duan et al., 2018).

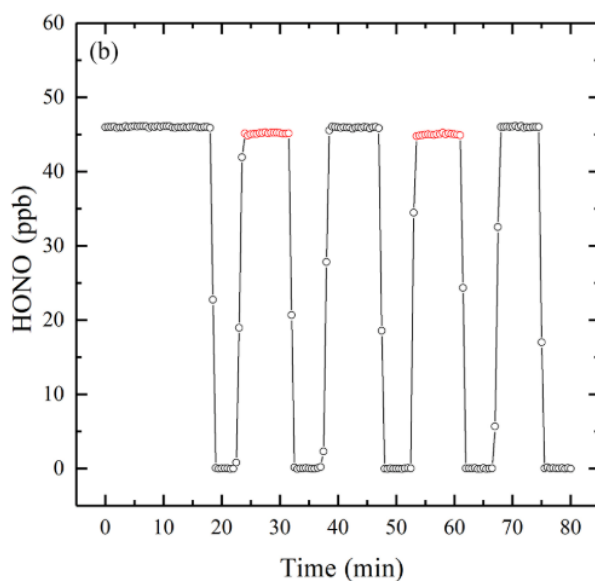


**Figure 1.** The black circles correspond to the HONO observed from the HONO standard generator. The red circle correspond to the HONO measured with the extra 1  $\mu$ m PTFE filter, 3 m PFA inlet tube and the simulative PFA optical cavity tube added in front of the IBBCEAS instrument.

7. Lines 178-183: This section needs clarification. Were these measurements made at all heights? Only on the ground? Or were these instruments located in the moving basket?

**Response:** Thanks for your comments. CO and O<sub>3</sub> were measured simultaneously at ground level and

at 260 m on the tower, while NO was measured only at ground level. We have made the clarification in the manuscript as the referee suggested.

*8. Line 184: In comparison to what? Clarify.*

**Response:** We have removed this sentence and added the accuracy of the instrument in the manuscript to make our statement more clearly.

*9. Line 202: Please add why use of these  $a$  and  $b$  terms are reasonable to use. The paper cited is for measurements made much further south, in the Pearl River Delta. A sound justification for the use of aerosol parameters from a location so far away, with far more agricultural impact on particulate composition (also different typical  $T$  and  $RH$ ).*

**Response:** As the referee suggested, we have made the clarification in the manuscript. The parameters  $a$  and  $b$  were derived using the measurement dataset from Guangzhou region, which, like Beijing, is one of the mega-cities in China. The curve-fitting parameters  $a$  (2.06) and  $b$  (3.6) for urban areas were used in the manuscript.

*10. Lines 213-219: Use all of these intercomparisons to determine some measure of relative accuracy between these four instruments (i.e. the relative standard deviation of the slopes).*

**Response:** We have modified this section and added the relative measurement difference between the four instruments.

*11. Line 235: 0.05 ppb is below the 1-sigma LOD. These low mixing ratios cannot be reported with any reliability. The Authors need to reconsider their interpretation anywhere that measurements are below 3-sigma LOD.*

**Response:** Thanks for the comment and suggestion. We have revised the manuscript as the referee suggested. The measurements below  $3\sigma$  LOD have been removed in the manuscript.

*12. Line 241: Delete 'other'*

**Response:** Revision has made as the referee suggested.

*13. Line 244: Which measurement or period these numbers correspond to is not clear. Please revise for clarity.*

**Response:** The sentence have been revised to make our statement more clearly.

*14. Line 264: +/- 0.4 ppb is very close to the 3-sigma detection limit, which suggests that these reported values may only be an evaluation of the difference in noise between the two instruments.*

**Response:** We have revised the discussion as the referee suggested.

*15. Lines 331-347: Apply corrections for Minor Comment 2 here and make changes throughout manuscript to match any alterations in the values of the slopes and their interpretation.*

**Response:** Revision has made as the referee suggested

*16. Lines 470-472: This should be calculated using the lower limit of the NO<sub>2</sub> mixing ratio (~40 ppbv) to provide a conservative estimate of the production rate. This reads as if the upper limit was used because it conveniently matched the observations, yet all of the remaining NO<sub>2</sub> measurements are below this value, which indicates that the aerosol surface conversion is a major contributor in isolated air parcels, but not the only contributor. This is more internally-consistent with the findings presented later in the manuscript where ground and aerosol surface contributions are compared throughout two nocturnal boundary layers after direct emissions are accounted for.*

**Response:** Thanks for the comment and suggestion. We calculated the HONO production using the average NO<sub>2</sub> mixing ratio (52.88 ppb) observed in the residual layer during E3. The absolute amount produced in an interval of 1.5 h could match the observations between vertical profile measurements (time interval: 1.5 h). As the referee pointed out, the aerosol surface dominates HONO production aloft by heterogeneous conversion of NO<sub>2</sub> during haze episodes, and surface production of HONO and direct emissions into the overlying air are minor contributors.

*17. Lines 472-474: This is a comparison between the calculation and the observations, yet it is not clear which numbers belong to the calculation and the observation here. Also, the Authors should normalize to a constant time interval (e.g. pptv per hour) for both the calculation and the observation numbers, since one interval given here is 1.5 hours and the other is 'between two vertical profile*

*measurements'. There are other instances of comparisons between calculations and observations from here onward that make following the results difficult, if not impossible.*

**Response:** Thanks for the comment and suggestion. As the referee suggested, we have revised this section to make our argument more clearly. The constant interval time for both the calculation and the observation was used for comparison between the calculation and the observation. The time interval of 1.5 h used in the calculation is same as the time interval between two vertical profile measurements (1.5 h). The statement throughout the section 3.4.2 have been revised to make our argument more clearly.

*18. Lines 481-482: The end of this sentence should be modified to indicate that ground production of HONO or direct emission into the surface layer are minor contributors, according to the results of the addressing the prior comments in this section.*

**Response:** Revision has made as the referee suggested.

*19. Line 487: The Authors should again emphasize the severe limitation of the number of transects in their dataset here. This haze event has not been characterized for how typical or atypical it may be in terms of chemical composition and so these results may not hold under a more thorough investigation of HONO formation in Beijing during other haze episodes, yet provides motivation to find out!*

**Response:** As the referee suggested, we have emphasized the limitation of the number of vertical profile data in our study.

*20. Lines 501-507: Upper limit used again here, should use lower limit. Calculated formation rates are in ppbv/hr while HONO increases are pptv between transects. Please use the same units for both values to make the comparison simple for your readers. Also clearly state what fraction of the total HONO production these calculated rates account for.*

**Response:** Thanks for the comment and suggestion. The average concentration of NO<sub>2</sub> observed in the residual layer were used in the calculation. As the referee suggested, we have revised the discussion of the comparison between the calculation and the observation to make our argument more clearly. The fraction of the calculated HONO production to the total HONO have been added in the manuscript as suggested.

21. Lines 510-516: *The clarity of writing here makes this challenging to follow. Given the limitations given in the discussion here, it would seem that this vertical transect was not a very good case study for analysis. It may be better to remove this from the discussion.*

**Response:** Thanks for the comment and suggestion. We have revised this section as the referee suggested.

22. Lines 521-522: *The Authors state 'presumably dominated', yet they performed a quantitative assessment. Give the calculated fraction of the observed total HONO production. Clearly state that it only applies for a limited number of transects over a short period of a given night.*

**Response:** The sentence has been revised as the referee suggested.

23. Lines 546-547: *The Zhang et al (2018) observation in Beijing during haze has a value much higher than given here. Is this a typo? If not, then this much higher observation should be moved to the next sentence. A period should precede 'However' as well, instead of a comma.*

**Response:** As the referee pointed out, this is not a typo. We have moved it to the next sentence as the referee suggested.

24. Line 559: *The Authors are creating confusion here. The aerosol surface conversion of HONO in the residual layer dominated its production in that layer, but this does not tell us anything about how important aerosol conversion is throughout the nighttime troposphere until it is compared in the following discussion of surface production. Revise this here to 'is an active HONO production mechanism during haze episodes' to improve accuracy and clarity.*

**Response:** Revision has made as the referee suggested.

25. Line 568: *Revise to use the lower limits calculated and/or give the mean with +/- corresponding to reach the upper and lower limits. This will give a much better picture of the chemistry in this very nice comparison section of the discussion.*

**Response:** Thanks for the comment and suggestion. As the referee suggested, we gave the upper limit and the lower limit, and the mean with +/- corresponding to reach the upper and lower limits.



26. Line 598: Again, only an upper limit is used here, yet a reactive uptake coefficient of  $10^{-6}$  is common to find in the literature. The lower limit or the entire range should be explored. The upper limit use here, again, suggests the Authors are more interested in the upper limit of aerosol conversion importance rather than providing a balanced perspective. Given their extremely limited dataset, caution in the interpretation of this data will make the results of this work more valuable for future comparisons. Please revise here and for the calculations moving forward through the remaining discussion.

**Response:** Thanks for the comment and suggestion. As the referee suggested, we considered the upper and lower limits of the uptake coefficient ( $1 \times 10^{-5}$ – $1 \times 10^{-6}$ ), the uptake coefficient of  $5 \times 10^{-6}$  was used in the calculation. We have modified the calculations here and in the discussion below, as the referee suggested.

27. Lines 609-610: And when the reactive uptake of  $\text{NO}_2$  is  $10^{-6}$ , then how does it compare? The Authors should provide the fraction of aerosol HONO production to the total calculated here to indicate its importance. It is only one third of the total, at the upper limit, which means it is important, but not dominant.

**Response:** Thanks for the comment and suggestion. Considering the upper and lower limits of the uptake coefficient of  $\text{NO}_2$ , the uptake coefficient of  $5 \times 10^{-6}$  was used in the calculation. As the referee suggested, we have provided the fraction of aerosol production of HONO to the total production of HONO, contributing about 20% of the production of HONO, suggesting that aerosol production of HONO is an important nocturnal HONO source.

28. Line 619: Revise this section according to manuscript changes throughout.

**Response:** As the referee suggested, we have revised the conclusion according to the changes in the manuscript.

#### **References:**

Duan, J., Qin, M., Ouyang, B., Fang, W., Li, X., Lu, K. D., Tang, K., Liang, S. X., Meng, F. H., Hu, Z. K., Xie, P. H., Liu, W. Q., and Häslner, R.: Development of an incoherent broadband cavity-enhanced

absorption spectrometer for in situ measurements of HONO and NO<sub>2</sub>, *Atmos. Meas. Tech.*, 11, 4531-4543, <https://doi.org/10.5194/amt-11-4531-2018>, 2018.

## **2. Response to Anonymous Referee #3**

### **General comments:**

*I feel that the authors have satisfactorily addressed most of my concerns. The only comment I have is regarding equation (4) and (5) on p. 16. The Authors state "the yield of the hydrolysis reaction assumes that HONO and HNO<sub>3</sub> are formed by equimolar disproportionation of two NO<sub>2</sub> molecules and immediately release HONO." (line 454-456) They further state that equations (4) and (5) have been modified to account for the disproportionation. However, the NO<sub>2</sub> uptake coefficients used are independent of any product yield for reaction (R2). I recommend deleting the above quoted sentence on line 454-456 since it does not have any bearing on equation (4) and (5). In fact, as mentioned in my first review of this paper. It is well established in the literature that hydrolysis of N<sub>2</sub>O<sub>4</sub> only occurs at ppm levels of NO<sub>2</sub>, when the 2NO<sub>2</sub> = N<sub>2</sub>O<sub>4</sub> equilibrium favors N<sub>2</sub>O<sub>4</sub> formation; those concentrations are not present in the air of Beijing.*

**Response:** Thanks for the comment and suggestion. The quoted sentence have been removed as the referee suggested.

1 **High resolution vertical distribution and sources of HONO and NO<sub>2</sub> in the**  
2 **nocturnal boundary layer in urban Beijing, China**

3  
4 **Fanhao Meng<sup>1,2</sup>, Min Qin<sup>1</sup>, Ke Tang<sup>1,2</sup>, Jun Duan<sup>1</sup>, Wu Fang<sup>1</sup>, Shuaixi Liang<sup>1,2</sup>, Kaidi Ye<sup>1,2</sup>,**  
5 **Pinhua Xie<sup>1,2,3,5</sup>, Yele Sun<sup>3,4,5</sup>, Conghui Xie<sup>4</sup>, Chunxiang Ye<sup>6</sup>, Pingqing Fu<sup>4,\*</sup>, Jianguo Liu<sup>1,2,3</sup>,**  
6 **Wenqing Liu<sup>1,2,3</sup>**

7 <sup>1</sup>Key Laboratory of Environmental Optics and Technology, Anhui Institute of Optics and Fine  
8 Mechanics, Chinese Academy of Sciences, Hefei, 230031, China

9 <sup>2</sup>University of Science and Technology of China, Hefei, 230027, China

10 <sup>3</sup>Center for Excellence in Regional Atmospheric Environment, Institute of Urban Environment,  
11 Chinese Academy of Sciences, Xiamen, 361021, China

12 <sup>4</sup>State Key Laboratory of Atmospheric Boundary Layer Physics and Atmospheric Chemistry, Institute  
13 of Atmospheric Physics, Chinese Academy of Sciences, Beijing, 100029, China

14 <sup>5</sup>University of Chinese Academy of Sciences, Beijing, 100049, China

15 <sup>6</sup>State Key Joint Laboratory of Environmental Simulation and Pollution Control, College of  
16 Environmental Sciences and Engineering, Peking University, Beijing, China

17 \*now at: Institute of Surface-Earth System Science, Tianjing University, Tianjing, 300072, China

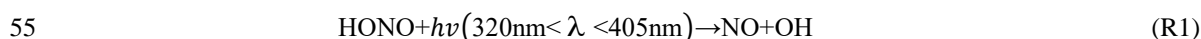
18 **Correspondence:** Min Qin (mqin@aiofm.ac.cn)

19  
20 **Abstract.** Nitrous acid (HONO), an important precursor of the hydroxyl radical (OH), plays a key role  
21 in atmospheric chemistry, but its sources are still debated. The production of HONO on aerosol surface  
22 or on ground surface in nocturnal atmospheres remains controversial. The vertical profile provides  
23 vertical information on HONO and NO<sub>2</sub> to understand the nocturnal HONO production and loss. In this  
24 study, we report the first high-resolution (<2.5 m) nocturnal vertical profiles of HONO and NO<sub>2</sub>  
25 measured from in-suit instruments on a movable container that was lifted on the side wiring of a 325-m  
26 meteorological tower in Beijing, China. High-resolution vertical profiles revealed the negative  
27 gradients of HONO and NO<sub>2</sub> in nocturnal boundary layers, and a shallow inversion layer affected the  
28 vertical distribution of HONO. The vertical distribution of HONO was consistent with stratification and  
29 layering in the nocturnal urban atmosphere below 250 m. The increase of HONO/NO<sub>2</sub> ratio was  
30 observed throughout the column from the clean episode to the haze episode, and a relatively constant

31 HONO/NO<sub>2</sub> ratios in the residual layer were observed during the haze episode. Direct HONO  
32 emissions from traffic contributed 29.3% ± 12.4% to the ambient HONO concentrations at night. The  
33 ground surface dominates HONO production by heterogeneous uptake of NO<sub>2</sub> during ~~the~~ clean  
34 episodes. In contrast, the HONO production ~~solely~~ on aerosols ~~surface~~ (30–300 ppt) explained the  
35 observed HONO increases (15–368 ppt) in the residual layer, suggesting that the aerosol surface  
36 ~~dominates HONO production aloft during haze episodes, while the surface production of HONO and~~  
37 ~~direct emissions into the overlying air are minor contributors. was the location where the HONO was~~  
38 ~~formed, which could presumably dominate the production of HONO aloft during the haze episode.~~  
39 Average dry deposition rates of 0.74 ± 0.31 and 1.55 ± 0.32 ppb h<sup>-1</sup> were estimated during the clean and  
40 haze episodes, implying that significant quantities of HONO could be deposited to the ground surface  
41 at night. Our results highlight ever-changing contributions of aerosol and ground surfaces in nocturnal  
42 HONO production at different pollution levels and encourage more vertical gradient observations to  
43 evaluate the contributions from varied HONO sources.

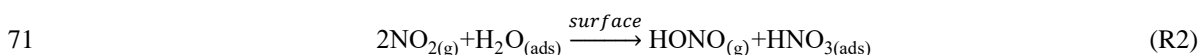
## 44 **1 Introduction**

45 It is well known that the rapid photolysis of nitrous acid (HONO) (R1) after sunrise is the most  
46 important hydroxyl radical (OH) source. 25%–60% of daytime OH production was accounted for due  
47 to HONO photolysis, according to previously reported (Lu et al., 2012; Ma et al., 2017; Tong et al.,  
48 2016; Su et al., 2008b; Huang et al., 2017; Spataro et al., 2013). OH initiates daytime photochemistry  
49 and promotes the formation of secondary products (including ozone (O<sub>3</sub>) and peroxyacetyl nitrate  
50 (PAN)) and secondary aerosols (Alicke and Platt, 2002; Tang et al., 2015; Kleffmann, 2007; An et al.,  
51 2012). In addition, HONO as a nitrosating agent forms carcinogenic nitrosamines (~~Sleiman et al., 2010;~~  
52 ~~Bartolomei et al., 2015; Gómez Alvarez et al., 2014~~) (Hanst et al., 1977; Pitts et al., 1978), and its  
53 health effects have attracted increasing amounts of concern (~~Hanst et al., 1977; Pitts et al., 1978~~)  
54 (Sleiman et al., 2010; Bartolomei et al., 2015; Gómez Alvarez et al., 2014).



56 Despite the importance of HONO, the details of the formation processes of HONO in the  
57 atmosphere are debated for decades. New state-of-the-art science instruments have observed much  
58 higher daytime HONO concentrations than simulated values from atmospheric chemical models in both  
59 rural and urban areas, implying missing HONO sources (Li et al., 2012; Wang et al., 2017; Oswald et

60 al., 2015; Wong et al., 2012; Li et al., 2014; Liu et al., 2019; Karamchandani et al., 2015; Kleffmann,  
61 2007; Mendez et al., 2017; Michoud et al., 2014; Michoud et al., 2015; Tang et al., 2015; Vogela et al.,  
62 2003; Sörgel et al., 2011). Several homogeneous reaction mechanisms for HONO have been proposed,  
63 but the latter have been considered as irrelevant under actual atmospheric conditions, including  
64 photolysis of ortho-substituted nitroaromatics (Bejan et al., 2006) and the reaction of photoexcited NO<sub>2</sub>  
65 with H<sub>2</sub>O (Li et al., 2008). The heterogeneous reduction of NO<sub>2</sub> with organic substrates is proposed to  
66 be another effective pathway to generate HONO (Brigante et al., 2008; Stemmler et al., 2006; George  
67 et al., 2005). However, extrapolation of lab results to real surfaces remains challenging. The nocturnal  
68 production of HONO has been considered to be dominated by the NO<sub>2</sub> heterogeneous reaction (R2).  
69 Although the heterogeneous reaction (R2) of HONO formation is first-order in NO<sub>2</sub>, the mechanism for  
70 the conversion of NO<sub>2</sub> on surfaces remains unclear (Finlayson-Pitts et al., 2003; Finlayson-Pitts, 2009).



72 A few studies have evaluated the relative importance of aerosol and ground surfaces in the  
73 nocturnal production of HONO via reaction (R2). The heterogeneous reaction on ground surface have  
74 been suggested as the primary nocturnal HONO source based on vertical measurements and fluxes in  
75 HONO (Harrison and Kitto, 1994; Harrison et al., 1996; Laufs et al., 2017; Kleffmann et al., 2003; Su  
76 et al., 2008b; VandenBoer et al., 2013; Villena et al., 2011; Wong et al., 2011; Wong et al., 2013; Stutz  
77 et al., 2002; Ye et al., 2017; Zhang et al., 2009). However, other ground level studies have found  
78 significantly positive correlations between HONO/NO<sub>2</sub> and aerosol surface areas, which suggests that  
79 the aerosols play an important role in the heterogeneous conversion of NO<sub>2</sub> to HONO (Reisinger, 2000;  
80 Cui et al., 2018; Zhang et al., 2018; Hou et al., 2016; Tong et al., 2016; An et al., 2012; Bao et al., 2018;  
81 Liu et al., 2014; Reisinger, 2000). Therefore, the primary reaction surfaces for the nighttime HONO  
82 formation is still controversial, and the role of the aerosols in the heterogeneous production of HONO  
83 remains an open question.

84 Vertical gradient observations provide evidence regarding surfaces and in situ HONO formation,  
85 which can help to understand the nighttime HONO sources. Methods of long-path differential optical  
86 absorption spectroscopy (LP-DOAS) (Stutz et al., 2002; Wong et al., 2011; Wong et al., 2012),  
87 instruments mounted on a movable elevator of a tall tower or a fixed height on a building (Kleffmann  
88 et al., 2003; VandenBoer et al., 2013; Villena et al., 2011) and aircraft measurements (Zhang et al.,

89 2009; Li et al., 2014; Ye et al., 2018) have been applied for HONO vertical gradient observations in  
90 Europe and the Americas. To determine the surface responsible for nocturnal HONO formation,  
91 Kleffmann et al. (2003) and Wong et al. (2011) measured the HONO vertical gradient between 10 and  
92 190 m altitude in a semi-rural area in Germany and at three different height intervals (lower: 20–70 m,  
93 middle: 70–130 m and upper: 130–300 m) in downtown Houston. Their consistent conclusion was that  
94 the reaction on the ground surfaces dominated the nocturnal formation of HONO. However, these types  
95 of measurements are limited by the measurement frequency or vertical resolution between the surface  
96 and the planetary boundary layer (PBL). VandenBoer et al. (2013) performed measurements of high  
97 resolution vertical profiles (vertical resolution ~10 m) of HONO on a 300-m tower. The total column  
98 observations of HONO also showed the ground as the dominant nocturnal surface on which HONO  
99 was generated from the heterogeneous reaction of NO<sub>2</sub>. The vertical information of HONO were  
100 interpreted in conjunction with a chemical model. The results suggested a conservative surface  
101 reservoir that was formed by the deposition of HONO could be a significant fraction of the unknown  
102 daytime source. Furthermore, in an attempt to understand the importance of HONO photochemistry in  
103 the troposphere, HONO gradients were measured in the PBL and the lower free troposphere (FT) over  
104 a forested region in Michigan (Zhang et al., 2009). An evaluation of the relative importance of aerosol  
105 and ground surfaces for the heterogeneous production of HONO also suggested that the ground surface  
106 was a major HONO source in the lower boundary layer. In addition, a substantial amount of daytime  
107 HONO existed in the FT (~8 ppt).

108 Beijing, as the largest and the most densely populated city in China, has suffered from severe haze  
109 pollution for several years due to rapid economic development and urbanization. Several ground-based  
110 observations of HONO have been conducted in urban and suburban areas of Beijing in recent years  
111 (Tong et al., 2016; Zhang et al., 2018; Hou et al., 2016; Wang et al., 2017; Lu et al., 2012; Hendrick et  
112 al., 2014). Higher levels of HONO have been observed (up to 9.71 ppb) in Beijing during winter  
113 (Spataro et al., 2013). Although few near real-time HONO vertical gradients have been made, and they  
114 have suggested that the reaction at the ground surface is the most important nighttime HONO source  
115 (Kleffmann et al., 2003; VandenBoer et al., 2013; Wong et al., 2012; Zhang et al., 2009). The relative  
116 importance of aerosol and ground surface in the production of nocturnal HONO may be different in the  
117 Beijing region. First, as the primary precursor of nighttime HONO, NO<sub>2</sub> has a much higher  
118 concentration during winter in Beijing due to the burning of fossil fuels and vehicle emissions. Second,

119 the aerosol surface area has been reported to be two to three orders of magnitude higher than the typical  
120 background area (Cai et al., 2017; Liu et al., 2012; Zhang et al., 2015). High aerosol surface area levels  
121 favor **aerosol surfaces to play** a heterogeneous **reactions on aerosol** surfaces (haze period:  $3000 \mu\text{m}^2$   
122  $\text{cm}^{-3}$ ; Wang et al., 2018), which presumably makes aerosol surfaces to play a more important role in the  
123 production of nighttime HONO. Third, there is more stable nocturnal stratification during the haze  
124 period in winter in Beijing, which may have influenced the vertical distribution of HONO. The  
125 contribution of the surface production of HONO to HONO levels aloft may be overestimated.

126 In this study, the first high-resolution vertical profile measurements of HONO and  $\text{NO}_2$  in the  
127 megacity of Beijing at different pollution levels (following the transition from a clean episode to a haze  
128 episode) are reported. The vertical profiles of HONO and  $\text{NO}_2$  are measured at high vertical resolution  
129 ( $< 2.5 \text{ m}$  over  $240 \text{ m}$  height) between the surface, the nocturnal boundary layer, and the residual layer.  
130 Although the vertical profile measurements are rather limited in scope, including only four nights in  
131 December 2016, with limited ancillary data, this study is unique due to the high vertical resolution  
132 obtained and due to the continuous HONO and  $\text{NO}_2$  vertical measurements obtained at different stages  
133 of pollution. The vertical profiles are then interpreted to evaluate the aerosol and ground surfaces  
134 responsible for the nighttime HONO formation during different pollution periods. The vertical  
135 measurements and simultaneous observations at ground level are then used to identify and quantify  
136 nighttime HONO sources.

## 137 **2 Experimental Methods**

### 138 **2.1 Measurement site**

139 Vertical profile measurements were conducted from December 7<sup>th</sup> to 12<sup>th</sup> of 2016 at the Tower  
140 Branch of the Institute of Atmospheric Physics (IAP), Chinese Academy of Science ( $39^\circ 58' \text{N}$ ,  
141  $116^\circ 23' \text{E}$ ) as part of the “In-depth study of air pollution sources and processes within Beijing and its  
142 surrounding region (APHH-Beijing)” winter campaign. The site is a typical urban residential area  
143 located between the 3<sup>rd</sup> and 4<sup>th</sup> Ring Road in the north of Beijing. It is approximately 1 km from the 3<sup>rd</sup>  
144 Ring Road, 200 m from the Beijing-Tibet Expressway, and 50 m from the Beitucheng West Road (Fig.  
145 S1). The primary sampling platform was the Beijing 325-m meteorological tower (BMT), equipped  
146 with an external container that was lifted on the side wiring of the tower, which could ascend and  
147 descend at a relatively constant rate of  $\sim 9 \text{ m min}^{-1}$ . A single vertical ascent or descent required less



148 than 30 min. After reaching the top, the container stopped and data were measured continuously for 5–  
149 20 min of each cycle. For security reasons, the container reached a maximum height limit of 260 m  
150 during the daytime and 240 m at night (Fig. 1). The container instruments included the following: a  
151 global position system (GPS), an altimeter, and an incoherent broadband cavity enhanced absorption  
152 spectrometer (IBBCEAS) for measurements of HONO and NO<sub>2</sub>. In addition, another IBBCEAS was  
153 mounted in temperature-stabilized lab containers for the measurement of HONO and NO<sub>2</sub> at ground  
154 level.

## 155 2.2 Instrumentation

156 HONO and NO<sub>2</sub> were simultaneously measured using a home-made IBBCEAS. A detailed  
157 description of the IBBCEAS instrument can refer to Duan et al (2018), and its application to the  
158 measurement made during this study is described below. IBBCEAS is a spectroscopic technique that  
159 combines broad-band light source (UV-LED) with the principle of time-integrated cavity output  
160 spectroscopy. The HONO was sampled into an inlet tube (1.5 m length with a 4 mm outside diameter  
161 (OD)) before entering an optical cavity (550 mm in length and 25.4 mm OD) that utilized PFA to  
162 minimize the HONO loss. The sampling gas flow rate was controlled at six standard liters per minute  
163 (SLPM) by a gas pump (KNF). In the optical cavity, light was reflected between the two highly  
164 reflective mirrors (R = 99.980% @368 nm, CRD Optics, California, USA) to obtain a long optical  
165 absorption length (the total optical path ~4.5 km). To protect the highly reflective mirrors, pure N<sub>2</sub> was  
166 used to continuously purge the mirrors to prevent contact between the mirrors and the sample airflow.  
167 The purge flow rate was controlled at 0.1 SLPM using mass flow controllers (MFCs, CS200A,  
168 Sevenstar, Beijing, China). The typical time resolution of the IBBCEAS instrument was 30 s, and the  
169 3  $\sigma$  detection limits for HONO and NO<sub>2</sub> were ~~99~~ 270 ppt and ~~470~~ 510 ppt, respectively. In this study,  
170 the IBBCEAS instrument was mounted in a movable container of the BMT for vertical profile  
171 measurements, and this made measurements with a time resolution of 15 s (vertical resolution of 2.4 m).  
172 The detection limits for HONO and NO<sub>2</sub> were ~~120~~ 360 ppt and ~~200~~ 600 ppt, respectively. Another  
173 IBBCEAS instrument was mounted in temperature-stabilized lab containers at ground level, and it  
174 collected data with a time resolution of 30 s. The total relative uncertainty of the IBBCEAS instrument  
175 was 8.7%, and it considered the uncertainty in the cross section (5%), the calibration of reflectivity  
176 (5%), spectral fitting (4%), the effective cavity length (3%), the pressure in the cavity (1%),  $\Delta I/I_0$

177 (1%), and sample loss (0.5%). Correction of the light intensity was performed every hour, and the  
178 mirror reflectivity was calibrated daily.

179 Meteorological parameters that included wind speed (WS), wind direction (WD), temperature ( $T$ ),  
180 and relative humidity (RH) were obtained using a 15-level meteorological gradient observation system  
181 installed at fixed intervals along the meteorological tower (at heights of 8, 15, 32, 47, 65, 80, 100, 120,  
182 140, 160, 180, 200, 240, 280, and 320 m). The gaseous species, including nitrogen monoxide (NO),  
183 ozone ( $O_3$ ), and carbon monoxide (CO) were measured using a commercial gas analyzer from Thermo  
184 Scientific (Waltham, Massachusetts, USA) (Tan et al., 2017). NO was detected using NO- $O_3$   
185 chemiluminescence (Model 42iTL, Thermo Scientific), with an accuracy of  $\pm 20\%$  and a detection limit  
186 of 50 ppt.  $O_3$  and CO were measured by an  $O_3$  analyzer (Model 49i, Thermo Scientific) and a CO  
187 analyzer (Model 48iTLE, Thermo Scientific), with the detection limits of 0.50 ppb and 0.04 ppm, and  
188 an  $O_3$  accuracy of  $\pm 20\%$ . ~~respectively. Measurements of NO,  $O_3$  and CO agreed well within the~~  
189 ~~instrumental accuracies.~~ The 7-wavelength aethalometer (AE33, Magee Scientific Corp, Berkeley,  
190 California, USA) was deployed to measure the black carbon (BC) at a time resolution of 1 min (Xie et  
191 al., 2019). Aerosol particles were continuously collected onto a quartz filter in the instrument to  
192 measure their light attenuation at 370, 470, 520, 590, 660, 880, and 950 nm. Trace gas (CO and  $O_3$ ) and  
193 aerosol parameters (BC, NR- $PM_{10}$  and aerosol surface area) were measured simultaneously at ground  
194 level and at 260 m on the tower, while NO was measured only at ground level. The non-refractory  
195 submicron aerosol (NR- $PM_{10}$ ) species were measured simultaneously at ground level and at 260 m  
196 using an aerodyne high-resolution time-of-flight aerosol mass spectrometer (AMS) and an aerosol  
197 chemical speciation monitor (ACSM), respectively. The detailed sampling setup and calibration of the  
198 AMS and ACSM, as well as data analysis, have been described by Xu et al. (2019) and Sun et al.  
199 (2013). The dry-state particle number size distributions were measured at ground level and at 260 m  
200 using a scanning mobility particle sizer (SMPS) (Du et al., 2017). The particle number size  
201 distributions of 15-500 nm was used to calculate the aerosol surface area ( $S_a$ ) by assuming the particles  
202 are in spherical shape. A hygroscopic factor  $f(RH)$  was applied to correct  $S_a$  to the aerosol surface area  
203 in the real atmosphere ( $S_{aw}$ ) (Li et al., 2012). The  $S_{aw}$  was calculated using following equations:

$$204 \quad f(RH) = 1 + a \left( \frac{RH}{100} \right)^b \quad (1)$$

$$205 \quad S_{aw} = S_a \times f(RH) \quad (2)$$

206 where  $a$  and  $b$  are the empirical fitting parameters used to estimate  $f(\text{RH})$ , which were set to 2.06 and  
207 3.6 in urban region, respectively (Liu et al., 2008). The curve-fitting parameters  $a$  and  $b$  were derived  
208 from the measurements in Guangzhou region, which, like Beijing, is one of the mega-cities in China.  
209 The uncertainty of  $S_{aw}$  was estimated to be ~30%, which was associated with the uncertainty from the  
210  $S_a$  measurement (~20%) and the growth factor (~20%).

### 211 2.3 Inter-comparison

212 In the present study, the measurements of HONO and  $\text{NO}_2$  were conducted simultaneously in the  
213 container and at ground level. Therefore, the calibration and inter-comparison of the two IBBCEAS  
214 instruments were crucial. Comparison experiments were conducted in a temperature-stabilized  
215 laboratory. The sampling unit and sampling flow rate of the two instruments were identical to minimize  
216 measured deviations. Figure. 2 shows the excellent agreement between the two IBBCEAS instruments  
217 (HONO:  $R^2 = 0.99$ ,  $\text{NO}_2$ :  $R^2 = 0.99$ ), with a slope of  $1.00 \pm 0.01$  ( $\text{NO}_2$ ),  ~~$1.02 \pm 0.01$~~   $1.00 \pm 0.01$   
218 (HONO) and a small intercept of  $180 \pm 90$  ppt ( $\text{NO}_2$ ) and  ~~$-30$~~   $-10 \pm 10$  ppt (HONO). The difference  
219 was approximately 2%, within the measurement error range of the instruments.

220 To verify the relative accuracy of the IBBCEAS instrument, an inter-comparison between the  
221 IBBCEAS of this study and the IBBCEAS of Cambridge University was conducted. The HONO  
222 measurements from the two different IBBCEAS instruments were highly consistent ( $R^2 = 0.97$  0.98,  
223 Fig. 2c), with a small intercept and a slope close to 1. The difference of 4% was within the range of the  
224 instrumental measurement error. In addition, the IBBCEAS instrument was also compared with the  
225 long optical path absorption photometer (LOPAP) and the stripping coil ion chromatography (SC-IC)  
226 from our previous studies (Tang et al., 2019; Duan et al., 2018). This also showed good agreements of  
227 the HONO measurements (LOPAP:  $R^2 = 0.894$ , SC-IC:  $R^2 = 0.98$ ). The regression slope and intercept  
228 of LOPAP to IBBCEAS was  $0.941 \pm 0.0069$  and  $0.110 \pm 0.0089$ , respectively, with a difference of ~6%.  
229 The linear regression of IBBCEAS against the SC-IC exhibited a slope of 0.82 with an intercept of 0.22.  
230 The difference of ~8% between the two instruments may be caused by the gas sampling.

## 231 3 Results and discussion

### 232 3.1 General observations and vertical measurements

233 The time-series of meteorological parameters, trace gases, and aerosol parameters are shown in  
234 Fig. 3. Based on the NR- $\text{PM}_{10}$  mass concentration level, three different meteorological conditions were

235 characterized during the measurement periods (Table 1). The first episode (E1) from December 7<sup>th</sup> to  
236 10:00 on December 8<sup>th</sup> was a haze event. The NR-PM<sub>1</sub> mass concentration increased rapidly from 30 to  
237 ~150 µg·m<sup>-3</sup> at ground level and at 260 m on the tower due to a low wind speed ( $0.78 \pm 0.42$  m·s<sup>-1</sup>) and  
238 a high RH ( $51\% \pm 13\%$ ).

239 The second episode (December 8-11, C2) was a clean event with low NR-PM<sub>1</sub> mass loading  
240 (mean:  $24 \pm 19$  µg·m<sup>-3</sup>) and a high wind speed ( $> 5$  m·s<sup>-1</sup>), primarily from northwest. The third episode  
241 (E3) from December 11<sup>th</sup> to December 12<sup>th</sup> was another haze event. During this period, the atmosphere  
242 was characterized by stagnant weather, lower wind speeds (an average of  $0.77 \pm 0.4$  m·s<sup>-1</sup>) and a high  
243 RH ( $55\% \pm 5\%$ ). The mass concentration of the NR-PM<sub>1</sub> gradually increased and then remained at  
244 relatively constant levels at ground level and 260 m on the tower, and ranging from 69 to 218 µg·m<sup>-3</sup>  
245 with a mean value of  $154 \pm 35$  µg·m<sup>-3</sup>.

246 Throughout the entire measurement periods, HONO concentrations ranged from ~~0.05~~ 0.27 to 7.59  
247 ppb. The mean HONO mixing ratios during E1, C2, and E3 were  $4.26 \pm 2.08$ , ~~0.83 ± 0.65~~  $0.90 \pm 0.65$ ,  
248 and  $3.54 \pm 0.91$  ppb, respectively. The maximum HONO concentration was 7.59 ppb, which was  
249 observed during E1 (at 08:10 on December 8<sup>th</sup>). From December 11<sup>th</sup> to 12<sup>th</sup> the pollutants continuously  
250 increased with the stagnant weather. The HONO concentrations remained at high levels, and the  
251 daytime mean HONO mixing ratio even reached  $3.10 \pm 0.92$  ppb. Figure 3 also shows the time series  
252 of simultaneously measured ~~other~~ relevant species. The mean NO<sub>2</sub> mixing ratios during E1, C2, and E3  
253 were  $51.98 \pm 8.41$ ,  $23.30 \pm 11.91$ , and  $51.88 \pm 5.97$  ppb, respectively. Because NO and O<sub>3</sub> were not  
254 measured at ground level after 14:00 on December 10<sup>th</sup>, the mean concentrations of NO and O<sub>3</sub> during  
255 E1 ~~and C2~~ were  $90.99 \pm 67.98$  and  $14.66 \pm 21.79$  ppb, ~~respectively, and~~ while the concentration of NO  
256 ~~and O<sub>3</sub> during C2~~ were  $4.04 \pm 1.81$  and  $14.37 \pm 10.65$  ppb, respectively. After sunset, the concentration  
257 of O<sub>3</sub> at the surface was rapidly titrated due to the elevated NO and increased with an increase in height.  
258 The mixing ratio of O<sub>3</sub> below 260 m was less than 9 ppb during the vertical measurements. The BC,  
259 NR-PM<sub>1</sub>, and aerosol surface area showed very similar patterns both at ground level and at 260 m. The  
260 RH corrected aerosol surface area ( $S_{aw}$ ) is shown in Fig. S2. Higher BC, NR-PM<sub>1</sub> and  $S_{aw}$  levels were  
261 observed at ground level during the haze periods (E1 and E3).

262 Nocturnal stable surface layers of air generally form at low wind speeds ( $< 6$  m·s<sup>-1</sup>) (VandenBoer  
263 et al., 2013). Hence, the vertical profile data were used when the wind speeds were less than 6 m·s<sup>-1</sup>,  
264 except on December 7<sup>th</sup>. Vertical measurements during low wind events were successfully conducted

265 on three occasions (December 9–10, 10–11, and 11–12) and will be discussed below. The  
266 near-continuous vertical measurements avoided the observation bias from prolonged fixed sampling.  
267 The date and time of the measurement for each vertical profile is detailed in Table S1 in the  
268 supplementary information.

### 269 **3.2 Nocturnal HONO vertical profiles**

#### 270 **3.2.1 Vertical measurements after sunset**

271 Vertical measurements were conducted from ground level to 240 m after sunset. The mixing ratios  
272 of HONO and NO<sub>2</sub> at ground level were consistent with those measured in the container. The mixing  
273 ratios of HONO and NO<sub>2</sub> showed nearly flat profiles throughout the column during C2 and E3 (Fig.  
274 S3), indicating that HONO and NO<sub>2</sub> were relatively well mixed after sunset. The vertical variations of  
275  $\Delta$ HONO, which is the difference in the HONO concentrations between measured in the container and  
276 at ground level, centered around 0 ppb. ~~and varied between 0.4 and 0.4 ppb.~~ **The variation of  $\Delta$ HONO**  
277 **throughout the column were close to the detection limit of the IBBCEAS instrument and were barely**  
278 **observed.** This result also indicated the relatively uniform vertical distribution of HONO. The vertical  
279 variations in *T* and RH during these three vertical measurements were similar (Fig. S4). While *T*  
280 decreased gradually with increasing height, RH increased gradually with increasing height. In addition,  
281 RH was relatively higher during the haze episode. Also, there was no *T* inversion just after sunset, and  
282 the consistent variations in the HONO and NO<sub>2</sub> at ground level and in the vertical measurements all  
283 supported a relatively well-mixed boundary layer, which explained the uniform vertical distribution of  
284 HONO and NO<sub>2</sub>.

#### 285 **3.2.2 Nocturnal vertical profiles**

286 Nocturnal small-scale stratification and layering was determined according to the method of  
287 Brown et al. (2012), who used the potential temperature profile as an indicator of atmospheric static  
288 stability. According to the vertical variations in the potential temperature, the stable layer was divided  
289 into the “surface layer”, the “nocturnal boundary layer (NBL)”, the “top of the nocturnal boundary  
290 layer”, and the “residual layer (RL)”.

291 Figure 4 depicts the nocturnal vertical profiles of HONO, NO<sub>2</sub>, and potential temperature during  
292 C2. The ~~orthogonal~~ linear least squares regression slope and correlation coefficients of HONO and NO<sub>2</sub>  
293 to altitude were applied to estimate the nocturnal gradient of HONO and NO<sub>2</sub> (Table 2). **Vertical profile**

294 data were used above the surface layer and 10 m vertical average from the surface to 240 m AGL to  
295 evaluate vertical gradient of HONO and NO<sub>2</sub>. An example of the regression line was shown in Fig. S5.  
296 On the night of December 9<sup>th</sup> (Fig. 4a), negative profiles of both HONO and NO<sub>2</sub> were clearly seen.  
297 When the container ascended during 22:42–23:06, the potential temperature profile showed distinct  
298 stratification. The surface layer extended to 10–20 m and the NBL extended to ~140 m. The obviously  
299 negative gradient of HONO (~~-4.49 ± 0.31~~ -4.56 ± 0.34 ppt m<sup>-1</sup>) and NO<sub>2</sub> (~~-14.38 ± 1.62~~ -16.41 ± 1.22  
300 ppt m<sup>-1</sup>) were observed throughout the heights from 0 to 240 m. A negative gradient of HONO was  
301 observed in the RL, but was not consistently observed in other measurements (see below). During the  
302 descent of the container from 23:15–23:40, the potential temperature profile showed that a shallow *T*  
303 inversion had rapidly formed between 130 and 200 m. The obvious vertical variation in RH during  
304 23:15–23:40 (Fig. S3) also indicated the different layers at different heights, which was due to the  
305 influence of a shallow inversion layer. Within the shallow inversion layer, vertical convection and  
306 transport were inhibited, and a remarkable negative gradient was observed there. However, within the  
307 NBL, the negative gradient of HONO and NO<sub>2</sub> disappeared. This might have been due to the  
308 continuous vertical mixing below the shallow inversion layer from 23:06 to 23:40. Additionally, the  
309 surface source of HONO was obvious, as evidenced by the apparently negative gradient of HONO in  
310 Table 2.

311 The vertical profile of potential temperature on December 10<sup>th</sup> (Fig. 4b) showed that a shallow  
312 inversion layer formed between the surface layer and the NBL. In the shallow inversion layer, the  
313 mixing ratios of HONO decreased rapidly with increasing height, and a significant negative gradient  
314 was observed within the shallow inversion layer and surface layer. With the attenuation of the shallow  
315 inversion layer during the descent of the container from 23:01 to 23:25, the inhibition of vertical  
316 transport and mixing gradually weakened. The increase in the negative gradient of HONO and NO<sub>2</sub> and  
317 the correlation coefficients of HONO and NO<sub>2</sub> to altitude from 22:36 to 23:25 also showed the  
318 weakened shallow inversion layer near the surface, which suggested the nighttime HONO surface  
319 source. The attenuation event of the shallow inversion layer may have also been the result of an  
320 increase in the wind speed and the interaction of different air masses that changed from the west to  
321 southeast between 15 and 100 m (Fig. S56). Above the 100 m height, the mixing ratio of HONO  
322 decreased with increasing height, and the fluctuation in HONO was likely due to the interaction of  
323 different air masses. In contrast, the vertical profiles of NO<sub>2</sub> showed that NO<sub>2</sub> rapidly decreased

324 towards the ground, and a significant positive gradient was observed near the surface that was caused  
325 by several factors. Nocturnal NO<sub>2</sub> is produced by the reaction of O<sub>3</sub> with NO, which primarily occurs  
326 near the surface, resulting in a negative gradient in NO<sub>2</sub>. However, this effect was counteracted by the  
327 dry deposition of NO<sub>2</sub>, which by itself would result in a positive gradient (Stutz et al., 2004b).  
328 Additionally, the mixing ratio of NO<sub>2</sub> was also affected by local traffic emission sources, and a  
329 near-surface shallow inversion layer was formed on December 10<sup>th</sup>. All of these presumably led to a  
330 clearly positive gradient for the near-surface NO<sub>2</sub>. In contrast to the vertical profiles measured on  
331 December 9<sup>th</sup>, a positive gradient observed in near-surface NO<sub>2</sub> on December 10<sup>th</sup> indicated that the  
332 shallow inversion layer affected the vertical distribution of HONO and NO<sub>2</sub> at night.

333 Although the surface layer was a common feature in the potential temperature profiles, it was  
334 absent during E3, and the NBL extended downward to the lowest measurement height (8 m above the  
335 ground). As shown in Fig. 5, the vertical profile of HONO showed a significant negative gradient as the  
336 container ascended during 22:35–23:00, and higher HONO mixing ratio was observed at ground level.  
337 With the development of the boundary layer, the negative gradient of HONO continued to decrease  
338 from  $6.91 \pm 0.33$   $6.92 \pm 0.36$  ppt m<sup>-1</sup> during 22:35–23:00 to  $1.79 \pm 0.28$   $1.98 \pm 0.28$  ppt m<sup>-1</sup> during  
339 00:45–01:09 and even disappeared between 00:00 and 00:26. Moreover, the consistent HONO/NO<sub>2</sub>  
340 ratios ( $\sim 5.6\% \pm 0.3\%$ ) were observed throughout the depth of the NBL between 23 and 01 h (Fig. S67).  
341 A near-steady state plateau of the HONO mixing ratio and HONO/NO<sub>2</sub> was established near midnight  
342 with the NBL. Similar vertical measurements were reported by VandenBoer et al (2013), who also  
343 observed a near-steady state in the HONO mixing ratio and HONO/NO<sub>2</sub>, and an approximate balance  
344 between the production and loss of HONO late in the night. A possible physical and chemical process,  
345 the loss of HONO to the ground surface due to dry deposition could account for the buildup and  
346 near-steady state observed in the HONO mixing ratio and HONO/NO<sub>2</sub>. This implied that significant  
347 quantities of HONO were deposited to the ground surface at night.

348 The utility of the [orthogonal](#) linear least squares regression slope of HONO to altitude to estimate  
349 the vertical gradient of HONO at night implies that the potential nocturnal HONO production from the  
350 heterogeneous reaction of NO<sub>2</sub> on aerosol surface. A positive gradient of HONO ( $0.23 \pm 0.36$   $0.24 \pm$   
351  $0.39$ ) between 00:00 and 00:26 was observed during E3. The aerosol surface area ( $S_{aw}$ ) in the residual  
352 layer was greater than 1500 μm<sup>2</sup> cm<sup>-3</sup> throughout the night (range: 1592-2655 μm<sup>2</sup> cm<sup>-3</sup>). The  $S_{aw}$  was  
353 2314 μm<sup>2</sup> cm<sup>-3</sup> from 22 to 01 h on December 11<sup>th</sup> and reached a maximum of 2569 μm<sup>2</sup> cm<sup>-3</sup> in the

354 residual layer. These aerosol surface areas are a factor of 14-38 greater than that observed in previous  
355 studies of HONO vertical gradient, which ranged between 60 and 158  $\mu\text{m}^2 \text{cm}^{-3}$  (Kleffmann et al., 2003;  
356 VandenBoer et al., 2013). Such high aerosol surface areas may provide a sufficient surface for the  
357 heterogeneous reaction. The vertical profiles also showed an enhanced HONO/NO<sub>2</sub> ratios from C2 to  
358 E3 (Fig. S78). Moreover, a relatively constant HONO mixing ratio and HONO/NO<sub>2</sub> ratio above 160 m  
359 were observed from 22:35 to 01:09 during E3. Both of these observations are indicative of a potential  
360 aerosol surface source of HONO aloft during the haze episode. Assuming that aerosol surface  
361 production dominated the observed HONO mixing ratio in the overlying air during the haze episode,  
362 the mixing ratios of HONO and NO<sub>2</sub> observed at 240 m and the aerosol surface area measured at 260 m  
363 were parameterized to estimate the nocturnal production of HONO on aerosol surface, which is  
364 explored in more detail in section 3.4.2.

### 365 **3.3 Direct emissions**

366 In the present study, the measurement site was surrounded by several main roads, and thus might  
367 have been affected by vehicle emissions. CO and NO, as the primary pollutants, are emitted from  
368 combustion processes like the burning of fossil fuels as well as vehicle emissions (Sun et al., 2014;  
369 Tong et al., 2016; Bond et al., 2013). BC is another primary pollutant typically emitted from diesel  
370 engines and residential solid fuels (Zhang et al., 2018). Good correlations of the nocturnal HONO with  
371 CO ( $R^2=0.85$ ), NO ( $R^2=0.76$ ) and BC ( $R^2=0.84$ ) at ground level were observed (Fig. S89), indicating  
372 the potential effect of direct emissions on the observed HONO at night. The emission ratio of  
373 HONO/NO<sub>x</sub> have been determined from tunnel measurements in California (Kirchstetter et al., 1996),  
374 Germany (Kurtenbach et al., 2001), and Hong Kong (Laing et al., 2017). However, considering the  
375 differences in the type of vehicles, fuel compositions, and other factors, the reported emission factor of  
376 HONO/NO<sub>x</sub> might not be representative for the Beijing region. To evaluate the influence of direct  
377 emissions, the local emission factor of HONO was derived from ambient measurements. Since NO was  
378 not measured at ground level after December 10<sup>th</sup>, the nighttime measurement data of HONO and NO<sub>x</sub>  
379 from November 9<sup>th</sup> to December 10<sup>th</sup> were used to evaluate the local HONO emission factor.

380 Considering the potential secondary HONO formation with air mass aging during the transport  
381 process, five criteria were applied to ensure as much of the freshly emitted air masses as possible: (a)  
382 only nighttime data (from 18:00 LT to next 6:00 LT) were included to avoid the fast photolysis of



383 HONO; (b) only sharp peaks during nighttime and the elevations of HONO and NO<sub>x</sub> over the  
384 background levels were estimated; (c)  $\Delta\text{NO}/\Delta\text{NO}_x > 0.80$ ; (d) good correlation between HONO and  
385 NO<sub>x</sub>; (e) short duration of the plume (< 30 min). The typical nighttime wind speed at measurement site  
386 was 1.2 m s<sup>-1</sup>, thus the duration for fresh air masses should have been less than 30 min during transport  
387 from the emission to the measurement site. Criteria (b) and (c) were used as indicators for identifying  
388 fresh vehicular emissions. Criteria (d) and (e) further confirmed that the increase in HONO was  
389 primarily caused by freshly emitted plumes instead of heterogeneous reactions of NO<sub>2</sub>.

390 Figure 6 shows two emission plumes observed on December 9<sup>th</sup> to 10<sup>th</sup>, 2016 based on the  
391 preceding selection criteria. The slopes of HONO to NO<sub>x</sub> can be considered as the emission ratios  
392 (Rappenglück et al., 2013). The HONO/NO<sub>x</sub> emission ratios were estimated for the 11 fresh emission  
393 plumes that satisfied the preceding criteria (see Table 3). The derived emission factors of 0.78%–1.73%  
394 had an average value of 1.28% ± 0.36%, which was larger than the 0.53%–0.8% measured in the tunnel  
395 in Wuppertal (Kurtenbach et al., 2001). The minimum ratio of 0.78% approximated the value (0.8%)  
396 measured in Wuppertal. It is worth mentioning that the value of 0.8% is widely used as the upper limit  
397 of the HONO/NO<sub>x</sub> emission ratio from road traffic in interpreting field observations and modeling  
398 HONO emissions (Stutz et al., 2002; Su et al., 2008a; Tong et al., 2016). The maximum ratio of 1.73%  
399 in this study is comparable to the value of 1.7% in Houston, Texas, observed by Rappenglück et al.  
400 (2013). The derived emission ratios were within the range of other published results (0.19%–2.1%)  
401 (Kirchstetter et al., 1996; Kurtenbach et al., 2001; Su et al., 2008a; Rappenglück et al., 2013; Yang et  
402 al., 2014; Xu et al., 2015; Liang et al., 2017; Zhang et al., 2018; Li et al., 2018; Liu et al., 2019).  
403 Comparisons of the derived HONO/NO<sub>x</sub> ratios with the results obtained previously are summarized in  
404 Table S2. To minimize the risk of overestimating the direct emissions, the minimum HONO/NO<sub>x</sub> ratio  
405 was used as an upper limit for the emission factor (Su et al., 2008a). The minimum HONO/NO<sub>x</sub> ratio of  
406 0.78% was used to evaluate the contribution of vehicle emissions to the ambient HONO levels at night  
407 (Eq. (3)). In this case, the risk of overestimating direct emissions was minimized, but there was still the  
408 effect of potential secondary HONO formation.

$$409 \quad [\text{HONO}]_{emis} = 0.0078 \times [\text{NO}_x] \quad (3)$$

410 where  $[\text{HONO}]_{emis}$  and  $[\text{NO}_x]$  are the HONO mixing ratios from vehicle emissions and the observed  
411 NO<sub>x</sub> mixing ratios, respectively. The direct emissions contributed an average of 29.3% ± 12.4% to the  
412 ambient HONO concentrations at night, with an average HONO<sub>emis</sub>/HONO value of 35.9% ± 11.8%

413 during the clean episode and an average  $\text{HONO}_{\text{emis}}/\text{HONO}$  value of  $26\% \pm 11.3\%$  during the haze  
414 episode. The frequency distribution of  $\text{HONO}_{\text{emis}}/\text{HONO}$  during the clean and the haze episodes are  
415 shown in Fig. 7. The lower vehicle emissions contribution during the haze episode could have been  
416 caused by an odd-even car ban, which required alternate driving days for cars with even- and  
417 odd-numbered license plates.

### 418 **3.4 Nocturnal HONO chemistry**

#### 419 **3.4.1 Correlation studies**

420 The heterogeneous conversion of  $\text{NO}_2$  is an important pathway for HONO formation during the  
421 nighttime, as many field observations have found a good correlation between HONO and  $\text{NO}_2$  (Zhou et  
422 al., 2006; Su et al., 2008a; Wang et al., 2013; Huang et al., 2017). However, the use of a correlation  
423 analysis to interpret the heterogeneous conversion of  $\text{NO}_2$  should be treated carefully, as physical  
424 transport and source emissions also contribute to the correlation. In this study, the correlations of  
425 vertical profiles between HONO and  $\text{NO}_2$  were analyzed. Vertical profile data without horizontal  
426 transport were used to avoid the influence of physical transport. As shown in Fig. 8, the linear least  
427 squares regression correlations of HONO to  $\text{NO}_2$  exhibited moderate but significant correlations (C2:  
428  $R^2 = 0.72$ , E3:  $R^2 = 0.69$ ), supporting that  $\text{NO}_2$  participated in the formation of HONO. The column of  
429 HONO and  $\text{NO}_2$  showed a significantly positive correlation during the haze episode. However, the  
430 negative correlation between HONO and  $\text{NO}_2$  was observed at ground level during the haze episode  
431 (Fig. S910), which was also observed in the previous ground-based observations (Hou et al., 2016;  
432 Zhang et al., 2018). The observed significant correlation between the HONO column and  $\text{NO}_2$  column  
433 could be due to: (1) emissions and vertical mixing of HONO and  $\text{NO}_2$ , and (2) a possible  
434 heterogeneous reaction of  $\text{NO}_2$  on aerosol surface.

435 Adsorbed water on a surface has been shown to affect the heterogeneous formation of HONO  
436 (Stutz et al., 2004a). The relationship between  $\text{HONO}/\text{NO}_2$  and RH is illustrated in Fig. 9. Following  
437 the method introduced by Stutz et al (2004a), the average of the five highest  $\text{HONO}/\text{NO}_2$  values in each  
438 10% RH interval was evaluated to eliminate much of the influence of factors like the time of night,  
439 advection, the surface density, etc. An increase in the  $\text{HONO}/\text{NO}_2$  ratio along with RH was observed at  
440 each height interval when the RH was less than 70%. A previous observation at ground level also  
441 reported that the  $\text{HONO}/\text{NO}_2$  ratio increased with an increase in RH when the RH was less than 70%. A

442 further increase in RH would lead to a decrease in the HONO/NO<sub>2</sub> ratio, which was considered to be  
443 caused by the number of water monolayers that formed on the surface leading to an efficient uptake of  
444 HONO (Li et al., 2012; Yu et al., 2009; Liu et al., 2019). However, a decreased uptake coefficient of  
445 HONO with increasing RH from 0% to 80% was observed in a laboratory study (Donaldson et al.,  
446 2014). The NO<sub>2</sub> to HONO conversion efficiency depended negatively on RH at an RH above 70%,  
447 which was presumably caused by the relative humidity affecting both HONO uptake onto the surface  
448 and the NO<sub>2</sub>-to-HONO conversion. A decrease in the HONO/NO<sub>2</sub> ratio with an increase in height at a  
449 similar RH level were observed during C2 and E3. A higher conversion efficiency of NO<sub>2</sub> to HONO  
450 was observed near the surface, and the HONO/NO<sub>2</sub> ratios at different heights were significantly  
451 different during C2. However, this differences decreased, and similar HONO/NO<sub>2</sub> ratios were observed  
452 at different heights during E3. This observation implied a possible heterogeneous conversion of NO<sub>2</sub> on  
453 aerosol surface in the overlying air. It is necessary to note that the limited vertical measurements  
454 resulted in a limited variation range in the RH, which limits this analysis. Additional efforts are needed  
455 to conduct more comprehensive vertical measurements to interpret the HONO/NO<sub>2</sub> ratios versus RH  
456 for different heights in the future.

#### 457 **3.4.2 Relative importance of aerosol and ground surfaces in nocturnal HONO production**

458 The observed positive HONO gradient implied a potential heterogeneous conversion of NO<sub>2</sub> on  
459 aerosol surface. The aerosol surface area observed during the haze episode was an order of magnitude  
460 higher than in other studies of HONO vertical gradient (Kleffmann et al., 2003; VandenBoer et al.,  
461 2013), which presumably provided sufficient aerosol surface area to account for the observed nighttime  
462 HONO production (Liu et al., 2019). The surface area information for particles larger than 0.5 μm were  
463 not valid at ground level and 260 m during the measurement periods. Hence, this is a lower limit  
464 estimate of the total surface area for the heterogeneous reaction.

465 An estimate of the nocturnal HONO production on aerosol surface was made using the RH  
466 corrected aerosol surface area ( $S_{aw}$ ) and NO<sub>2</sub> observations from the residual layer. The CO and BC  
467 measured at ground level were independent of the CO and BC observed at 260 m during the haze  
468 period (Fig. S1011), since it can be expected that air masses in the residual layer were decoupled from  
469 the ground-level processes and largely free of NO<sub>2</sub> emissions. (Brown et al., 2012; VandenBoer et al.,  
470 2013). The HONO production from the heterogeneous NO<sub>2</sub> conversion (Reaction R1) on aerosol

471 surface would then have become the primary HONO source in the residual layer during E3. ~~The yield~~  
 472 ~~of the hydrolysis reaction assumes that HONO and HNO<sub>3</sub> are formed by equimolar disproportionation~~  
 473 ~~of two NO<sub>2</sub> molecules and immediately release HONO (Finlayson Pitts et al., 2003; Finlayson Pitts,~~  
 474 ~~2009).~~ The reactive uptake of NO<sub>2</sub> by the aerosols was assumed to occur on all measured aerosol  
 475 surface areas, regardless of their chemical composition. HONO production ( $P(HONO)$ ) can then be  
 476 expressed using the equation of Ye et al. (2018) modified to account for the disproportionation:

$$477 \quad \frac{P(HONO)}{[NO_2]} = \frac{1}{8} \times S_{aw} \times \sqrt{\frac{8RT}{\pi M}} \times \gamma_{NO_2} \quad (4)$$

478 where  $\gamma_{NO_2}$  is the uptake coefficient,  $R$  is the gas constant,  $T$  is the absolute temperature (K),  $M$  is the  
 479 molecular mass of NO<sub>2</sub> ( $M=4.6 \times 10^{-2}$  kg mol<sup>-1</sup>), and  $S_{aw}$  is the RH corrected aerosol surface area ( $\mu\text{m}^2$   
 480 cm<sup>-3</sup>). The NO<sub>2</sub>-normalized HONO production over time,  $\Delta \frac{[HONO]}{[NO_2]}/\Delta t$ , can be calculated using the  
 481 following Eq. (5):

$$482 \quad \Delta \frac{[HONO]}{[NO_2]}/\Delta t \sim \frac{1}{8} \times S_{aw} \times \sqrt{\frac{8RT}{\pi M}} \times \gamma_{NO_2} \quad (5)$$

483 Assume an NO<sub>2</sub> uptake coefficient of  $1 \times 10^{-5}$  to  $1 \times 10^{-6}$  in the dark, which fits the NO<sub>2</sub> uptake  
 484 coefficient values observed in relevant studies (J.Kleffmanna et al., 1998; Kurtenbach et al., 2001;  
 485 Saastad et al., 1993; Bröske et al., 2003). A representative temperature of 273 K, and an average observed  
 486  $S_{aw}$  of 2314  $\mu\text{m}^2$  cm<sup>-3</sup> in the residual layer between 22 and 01 h during E3 were used. A relative HONO  
 487 accumulation rate of  $\Delta \frac{[HONO]}{[NO_2]}/\Delta t$  ranged between 0.00037 and 0.0037 h<sup>-1</sup>, equivalent to the HONO  
 488 production of 0.02 to 0.20 ppb h<sup>-1</sup> at a constant NO<sub>2</sub> concentration of 54 52.88 ppb, which was the  
 489 ~~average value upper limit~~ of the ~~observed~~ nocturnal NO<sub>2</sub> ~~observed~~ in the residual layer during E3. ~~The~~  
 490 ~~produced HONO amount of 30–300 ppt in an interval of 1.5 h could account for the HONO increases~~  
 491 ~~of 15–368 ppt in the residual layer between the two vertical profile measurements. The absolute~~  
 492 ~~amount produced of HONO in an interval of 1.5 h (30–300 ppt) could account for the observed~~  
 493 ~~increases of HONO (15–368 ppt) in the residual layer between vertical profile measurements on~~  
 494 ~~December 11<sup>th</sup> (time interval: 1.5 h).~~ Thus, production from the heterogeneous conversion of NO<sub>2</sub>  
 495 ~~solely~~ on aerosol surface can explain the HONO observations during E3. In addition, if the HONO  
 496 production aloft was indeed dominated by reactions on aerosol surface, the column average  
 497 concentration of HONO would be expected to be independent of the amount of HONO observed at  
 498 ground level. Figure 10a shows that the column of HONO is independent of the mixing ratio of HONO

499 observed from the ground level to 10 m in height ( $R^2 = 0.27$ ), which is consistent with the hypothesis  
500 that the aerosol surface ~~presumably~~ dominates HONO production aloft by heterogeneous uptake of  
501  $\text{NO}_2$  during the haze episode, and the production of HONO at ground level ~~and direct HONO emissions~~  
502 ~~is not transported to~~ into the overlying air ~~are minor contributors~~. This result was contrary to previous  
503 observations that the production of HONO on aerosol surface was insignificant compared to the ground  
504 surface (Kleffmann et al., 2003; Wong et al., 2011; VandenBoer et al., 2013), which could have been  
505 due to the higher aerosol surface area observed in this study. An order of magnitude higher aerosol  
506 surface area in the residual layer than in previous vertical observations ( $<160 \mu\text{m}^2 \text{cm}^{-3}$ ) was observed,  
507 which could provide sufficient aerosol surface area for the heterogeneous formation of HONO.  
508 ~~However, the limited vertical profile dataset limits a comprehensive investigation of HONO formation~~  
509 ~~in Beijing, yet provides a data basis and research direction.~~

510 An estimate of HONO production from the heterogeneous conversion of  $\text{NO}_2$  on aerosols was also  
511 made during C2 using  $S_{aw}$  and  $\text{NO}_2$  observations from the residual layer. The column of the average  
512 HONO concentration was related to the amount of HONO observed between ground level and 10 m  
513 (Fig. 10b,  $R^2 = 0.93$ ), suggesting that the surface HONO sources affected the HONO observed  
514 throughout the depth of boundary layer during C2. A high correlation ( $R^2 = 0.83$ ) between the measured  
515 CO and BC at ground level and the CO and BC at 260 m was also observed (Fig. S10), which indicated  
516 that vehicle emissions affected air masses in the residual layer. The lack of the NO vertical profile  
517 cannot directly correct the influence of direct HONO emissions. If it is assumed that the contribution of  
518 direct HONO emissions was consistent at ground level and in the residual layer, the relative  
519 contribution of the aerosol and ground surfaces to nocturnal HONO production in the residual layer  
520 could be roughly estimated during C2. The direct emissions contribution of  $35.9\% \pm 11.8\%$  during C2  
521 is a higher limit estimate of the contribution of direct emissions to the HONO levels in the residual  
522 layer.

523 The averages  $S_{aw}$  of 791 and  $894 \mu\text{m}^2 \text{cm}^{-3}$  from 17 to 24 h, and ~~an upper limit of the average~~  $\text{NO}_2$   
524 ~~mixing ratio observations~~ of ~~36~~ 34.67 and ~~44~~ 42.40 ppb from the residual layer were used to estimate  
525 HONO production on aerosol surface on December 9<sup>th</sup> and 10<sup>th</sup>. The formation rates of HONO on  
526 aerosol surface were ~~0.0047–0.047~~ 0.0045–0.045 ppb  $\text{h}^{-1}$  on the 9<sup>th</sup> and ~~0.0062–0.062~~ 0.0059–0.059  
527 ppb  $\text{h}^{-1}$  on the 10<sup>th</sup>. The ~~observed~~ HONO increased by 305–608 ppt between ~~vertical~~ profile  
528 measurements (time interval: 5.5 h), which have the contributions from direct HONO emissions

529 subtracted, were higher than the production of HONO (~~26–259~~ 25–248 ppt) in ~~the~~ an interval of 5.5 h  
530 on December 9<sup>th</sup>. The formation of HONO on aerosol surface cannot explain the observed HONO  
531 increases in the residual layer, which suggests that the HONO observed in the residual layer was  
532 primarily derived from the heterogeneous conversion of NO<sub>2</sub> on the ground surface followed by  
533 vertical transport throughout the column. ~~The aerosol production of HONO could account for up to~~  
534 ~~about 40% of HONO observations in the residual layer.~~ The HONO production from the aerosol  
535 surface in ~~the~~ an interval of 5.35 h was ~~33–332~~ 32–316 ppt ~~in the residual layer~~ on December 10<sup>th</sup>,  
536 which was comparable to the corrected HONO increases of 114–369 ppt ~~observed~~ between ~~vertical~~  
537 profile measurements (~~time interval: 5.35 h~~). A shallow inversion layer formed near the surface could  
538 account for the aerosols ~~surfaces play a heterogeneous reaction surface presumably dominated HONO~~  
539 ~~production~~ in the residual layer, ~~and this could have been due to the following: (1) the inhibition of~~  
540 ~~vertical transport of nighttime HONO source at ground level, and/or (2) an overestimation of the~~  
541 ~~contribution from direct HONO emissions to HONO concentrations in the residual layer.~~

542 In conclusion, HONO production solely on aerosol surface accounted for the HONO observations  
543 during E3. The ground surface dominated HONO production by heterogeneous conversion of NO<sub>2</sub>  
544 during the clean episode, which was then transported throughout the column. With the increases in the  
545 NO<sub>2</sub> mixing ratio and aerosol surface areas from the clean episode to the haze episode, the aerosol  
546 surface production became an important nocturnal source of HONO and ~~presumably~~ dominated the  
547 heterogeneous production of HONO aloft from NO<sub>2</sub> during the haze episode.

### 548 3.4.3 Nocturnal HONO production and loss at ground level

549 The nocturnal HONO observed throughout the depth of the boundary layer is primarily from the  
550 heterogeneous conversion of NO<sub>2</sub> on the ground surface during ~~the~~ clean episodes. The HONO  
551 conversion frequency can be estimated using the data from the nocturnal measurements at ground level  
552 (18:00–06:00 LT). The heterogeneous formation of HONO in reaction (R2) is first order in NO<sub>2</sub>, and  
553 the HONO formation is proportional to the NO<sub>2</sub> concentration. The conversion frequency was derived  
554 using the method proposed by Alicke et al. (2002). The emission ratio of HONO/NO<sub>x</sub> derived in  
555 section 3.3 was used to correct the HONO concentration by Eq. (6). Because NO was not measured at  
556 ground level after 14:00 on December 10<sup>th</sup>, the NO<sub>x</sub> data was not available during the nocturnal vertical  
557 measurements on December 10<sup>th</sup> and 11<sup>th</sup>. The average HONO<sub>emis</sub>/HONO ratio of 35.9% ± 11.8% and

558 26%  $\pm$  11.3% were used to correct the observed HONO concentrations (i.e.  $[HONO]_{corr} =$   
 559  $[HONO] - [HONO]_{emis}$ ) during the clean and the haze episodes after December 10<sup>th</sup>, respectively. The  
 560 NO<sub>2</sub>-to-HONO conversion frequency,  $k_{HONO}$ , can be calculated using Eq. (7), by assuming that  
 561 observed HONO comes from the conversion of NO<sub>2</sub> (Su et al., 2008a).

$$562 \quad [HONO]_{corr} = [HONO] - [NO_x] \times 0.0078 \quad (6)$$

$$563 \quad k_{HONO} = \frac{[HONO_{corr}]_{t_2} - [HONO_{corr}]_{t_1}}{(t_2 - t_1)[\overline{NO_2}]} \quad (7)$$

564 where  $[\overline{NO_2}]$  is the average NO<sub>2</sub> mixing ratio during the time interval of  $t_2 - t_1$ . The conversion  
 565 frequencies,  $k_{HONO}$ , on December 9<sup>th</sup>, 10<sup>th</sup>, and 11<sup>th</sup> were 0.0082, 0.0060 and 0.0114 h<sup>-1</sup>, respectively,  
 566 corresponding to a HONO production rate by NO<sub>2</sub> ( $P_{NO_2}$ ) of  $0.25 \pm 0.03$ ,  $0.28 \pm 0.02$ , and  $0.60 \pm 0.02$   
 567 ppb h<sup>-1</sup> (i.e.  $C_{HONO} \times [\overline{NO_2}]$ ), respectively. It is necessary to elaborate that the derived  $P_{NO_2}$  is the net  
 568 HONO production, which means sources and sinks of HONO (aerosol and ground surface sources,  
 569 deposition, etc.) have already been taken into account in the  $P_{NO_2}$ . The HONO conversion frequency  
 570 obtained in this study is comparable to the observations by Hou et al. (2016) (clean episode: 0.0065 h<sup>-1</sup>,  
 571 haze episode: 0.0039 h<sup>-1</sup>) and Zhang et al. (2018) in the Beijing region (haze episode: 0.058 h<sup>-1</sup>; ~~severe~~  
 572 ~~haze episode: 0.0146 h<sup>-1</sup>~~). However, they are lower than the observations made by Zhang et al. (2018)  
 573 ~~during the severe haze episode in Beijing (0.0146 h<sup>-1</sup>)~~, Li et al. (2012) ( $0.024 \pm 0.015$  h<sup>-1</sup>) and Su et al.  
 574 (2008b) ( $0.016 \pm 0.014$  h<sup>-1</sup>) at a rural site in southern China.

575 It was assumed that production of HONO on aerosol surface was insignificant compared to the  
 576 ground surface during the clean episode, which has been suggested in other studies of HONO vertical  
 577 gradient (VandenBoer et al., 2013; Wong et al., 2011; Zhang et al., 2009). Therefore, the HONO  
 578 production ( $P_{NO_2}$ ) could be considered as a net contribution of the surface production of HONO to the  
 579 total column of HONO when HONO deposition is considered in  $P_{NO_2}$ . The surface production rate of  
 580 HONO of  $0.25 \pm 0.03$  and  $0.28 \pm 0.02$  ppb h<sup>-1</sup> were an order of magnitude higher than the maximum  
 581 production rate of HONO on aerosol surface (0.047 and 0.062 ppb h<sup>-1</sup>) on December 9<sup>th</sup> and 10<sup>th</sup>. This  
 582 result suggests that ground surface dominated HONO production by heterogeneous conversion of NO<sub>2</sub>  
 583 during the clean episode. In contrast, the production of HONO solely on aerosol surface can explain the  
 584 HONO observations in the residual layer during E3, indicating that the aerosol surface production was  
 585 ~~an important nocturnal source of HONO during the haze episodes~~ **an active HONO production**  
 586 **mechanism during haze episodes**. The derived  $P_{NO_2}$  is the total HONO production rate of the aerosol

587 and ground surfaces by heterogeneous conversion of NO<sub>2</sub>. To compare the HONO heterogeneous  
 588 production on aerosol and ground surfaces, a deposition velocity of NO<sub>2</sub> to the surface in the dark,  
 589  $V_{dep,NO_2}$ , of 0.07 cm s<sup>-1</sup> (VandenBoer et al., 2013), in a boundary layer of height,  $h$  of 140 m, was used  
 590 to estimate the HONO production rate by NO<sub>2</sub> on the ground surface. The nocturnal production of  
 591 HONO by heterogeneous uptake of NO<sub>2</sub> on ground surface can be estimated by the following,

$$592 \quad P_{HONO,ground} = \frac{1}{2} \frac{V_{dep,NO_2}}{h} \overline{[NO_2]} \quad (8)$$

593 The surface production rate of HONO ( $P_{HONO,ground}$ ) was  $0.47 \pm 0.02$  ppb h<sup>-1</sup> on December 11<sup>th</sup> (E3),  
 594 which was comparable to the HONO production rate on aerosol surface of 0.02–0.2 ( $0.11 \pm 0.09$ ) ppb  
 595 h<sup>-1</sup>. This result also suggests that the production of HONO on aerosols is an important nocturnal source  
 596 of HONO during the haze episodes. The higher production rates of HONO on the ground surfaces were  
 597 consistent with the fact that the ground had a much greater surface area than the aerosol (i.e., the ground  
 598 surface area was 7140 μm<sup>2</sup> cm<sup>-3</sup> in a 140 m deep NBL, versus the average  $S_{aw}$  of 2255 μm<sup>2</sup> cm<sup>-3</sup> during  
 599 E3). However, the vertical transport of the surface production of HONO throughout the column was  
 600 likely inhibited during E3. The column average concentration of HONO was independent of the mixing  
 601 ratio of HONO observed between ground level and 10 m (Fig. 10a), which may have been due to a  
 602 more stable nocturnal boundary layer structure during the haze episode.

603 A budget equation of nighttime HONO (Eq. 9) was utilized to separate the contributions of the  
 604 individual chemical processes involved in the nocturnal production and loss of HONO (Su et al., 2008b;  
 605 Oswald et al., 2015).

$$606 \quad \frac{d[HONO]}{dt} = P_{emis} + P_{aerosol} + P_{ground} + P_A - L_{dep} \pm T_h \pm T_v \quad (9)$$

607 The production terms of the HONO consist of the direct emission rate ( $P_{emis}$ ); the heterogeneous  
 608 production rate on aerosol ( $P_{aerosol}$ ) and ground surfaces ( $P_{ground}$ ); and the additional nighttime  
 609 HONO source/sink ( $P_A$ ). The loss process ( $L_{dep}$ ) is the dry deposition rate at nighttime.  $T_h$  and  $T_v$   
 610 describe the horizontal and vertical transport processes, respectively. The horizontal transport,  $T_h$ , is  
 611 negligible in a relative calm atmosphere with low wind speeds (<1.6 m s<sup>-1</sup>) during vertical  
 612 measurements. The vertical transport,  $T_v$ , acts as a sink close to the surface and as an additional source  
 613 at elevated levels. However, it is difficult to quantify  $T_v$  without direct measurements of fluxes or  
 614 using the chemical transport model, and its contribution is uncertain. Without explicitly considering  $T_v$ ,  
 615 the budget analysis is reasonable for relatively well-mixed conditions. Thus, the budget analysis is used



616 for the measurements conducted on December 9<sup>th</sup> and 10<sup>th</sup>, when no shallow inversion layer was  
 617 observed near the surface.

618 Simplifying Eq. (9), the  $dHONO/dt$  was approximated by  $\Delta HONO/\Delta t$ , which is the difference  
 619 in the observed HONO mixing ratios at two time points. An additional nocturnal production rate term  
 620 ( $P_A$ ) can be derived by Eq. (10). The emission ratio of HONO/NO<sub>x</sub> (0.78%) and HONO<sub>emis</sub>/HONO ratio  
 621 ( $26\% \pm 11.3\%$ ) obtained in section 3.3 were used to estimate  $P_{emis}$ . The nocturnal production of  
 622 HONO via NO<sub>2</sub> on aerosol and ground surfaces, and the production rate terms of  $P_{aerosol}$  and  
 623  $P_{ground}$  in Eq. (4) and (8) were used as representations of the nocturnal production of HONO in Eq.  
 624 (10). Here, with an overall consideration of uptake coefficient of  $\gamma_{NO_2}$  used in the literature, An upper  
 625 limit uptake coefficient of the  $\gamma_{NO_2}$  ( $1 \times 10^{-5}$ ) was assumed to be  $5 \times 10^{-6}$  to estimate the HONO  
 626 production rate on aerosol surface. For  $L_{dep}$ , the temperature-dependent deposition velocity of HONO  
 627 ( $(V(HONO))_T = \exp(23920/T - 91.5)$ ) was used to estimate the  $V_{dep,HONO}$ , which decreased  
 628 exponentially to non-significant values at 40 °C (Laufs et al., 2017). The average  $V_{dep,HONO}$  calculated  
 629 from the nocturnal measurements (00:00–06:00 LT) was 1.8 cm s<sup>-1</sup>, with a range of values spanning 0.9  
 630 to 3 cm s<sup>-1</sup>, which was within the range of previously reported values between 0.077 and 3 cm s<sup>-1</sup>  
 631 (Harrison and Kitto, 1994; Harrison et al., 1996; Spindler et al., 1998; Stutz et al., 2002; Coe and  
 632 Gallagher, 1992; Laufs et al., 2017).

$$633 \quad \frac{\Delta HONO}{\Delta t} = \frac{1}{2} \frac{V_{dep,NO_2}}{h} [NO_2] + \frac{1}{8} S_{aw} C_{NO_2} \gamma_{NO_2} [NO_2] + \frac{\Delta HONO_{emis}}{\Delta t} + P_A - \frac{V_{dep,HONO}}{h} [HONO] \quad (10)$$

634 Figure 11 shows the nocturnal HONO budgets from 18:00 to 06:00 LT on the 9<sup>th</sup> (C2) and 11<sup>th</sup> (E3)  
 635 of December. The production rate of HONO on aerosol surface ( $0.04 \pm 0.01$   ~~$0.02 \pm 0.01$~~  ppb h<sup>-1</sup>) was  
 636 insignificant compared to the ground surface ( $0.28 \pm 0.03$  ppb h<sup>-1</sup>) during C2. However, an average  
 637  $P_{aerosol}$  of  ~~$0.19 \pm 0.01$~~   $0.10 \pm 0.01$  ppb h<sup>-1</sup> derived during E3 was comparable to the surface production  
 638 rate of HONO ( $P_{ground}$ ,  $0.47 \pm 0.03$  ppb h<sup>-1</sup>), contributing about 20% of the production of HONO,  
 639 which supported supporting the preceding result that HONO production on aerosols was an important  
 640 nocturnal source of HONO during the haze episode. For the source of direct HONO emissions,  $P_{emis}$   
 641 only just provided a small portion part of the HONO at a rate of  $0.06 \pm 0.07$  and  $0.10 \pm 0.10$  ppb h<sup>-1</sup>.  
 642 The loss of HONO due to surface deposition was the dominant sink for HONO during nighttime. The  
 643  $L_{dep}$  contributed  $0.74 \pm 0.31$  and  $1.55 \pm 0.32$  ppb h<sup>-1</sup> to the nocturnal loss of HONO during C2 and E3,  
 644 respectively, implying that significant amounts of HONO were deposited to the ground surface at night.

645 This had been suggested in another study on the vertical gradient of HONO (VandenBoer et al., 2013).

#### 646 **4 Conclusions**

647 High-resolution vertical profiles of HONO and NO<sub>2</sub> were measured using an IBBCEAS  
648 instrument during the APHH-Beijing winter campaign. To the best of our knowledge, this is the first  
649 high-resolution vertical measurements of HONO and NO<sub>2</sub> in urban areas of China. The HONO  
650 concentrations observed during E1, C2, and E3 were  $4.26 \pm 2.08$ ,  ~~$0.83 \pm 0.65$~~   $0.90 \pm 0.65$ , and  $3.54 \pm$   
651  $0.91$  ppb, respectively. A relatively well-mixed boundary layer was observed after sunset, and the  
652 vertical distribution of HONO was consistent with reduced mixing and stratification in the lower  
653 several hundred meters of the nocturnal urban atmosphere. The small-scale stratification of the  
654 nocturnal atmosphere and the formation of a shallow inversion layer affected the vertical distribution of  
655 HONO and NO<sub>2</sub>. A near-steady state in HONO mixing ratio and HONO/NO<sub>2</sub> ratio was observed near  
656 midnight on December 11<sup>th</sup> to 12<sup>th</sup>, and an approximate balance was established between the production  
657 and loss of HONO.

658 Direct HONO emissions contributed an average of  $29.3\% \pm 12.4\%$  to the ambient HONO levels at  
659 night. High-resolution vertical profiles of HONO revealed (1) the ground surface dominated HONO  
660 production by heterogeneous conversion of NO<sub>2</sub> during ~~the~~ clean episodes, (2) the production ~~solely of~~  
661 **HONO** on aerosols ~~surface~~ explained the HONO observations in the residual layer during E3,  
662 suggesting that the aerosols ~~production~~ was an important nighttime HONO source during ~~the~~ haze  
663 episodes. The column average HONO concentration was irrelevant to the HONO observed between the  
664 ground level and 10 m during E3, implying that the aerosols ~~presumably~~ ~~dominates~~ the heterogeneous  
665 production of HONO aloft from NO<sub>2</sub> during ~~the~~ haze episodes, **while the surface production of HONO**  
666 **and direct emissions into the overlying air are minor contributors**. Average dry deposition rates of  $0.74$   
667  $\pm 0.31$  and  $1.55 \pm 0.32$  ppb h<sup>-1</sup> were identified during the clean and haze episodes, respectively,  
668 implying that significant amounts of HONO were deposited to the ground surface at night. Overall,  
669 these results draw a picture of the nocturnal sources of HONO during different pollution levels, and  
670 demonstrated the urgent need for high-resolution vertical measurements of HONO to a high height (e.g.,  
671 using tethered balloons) and more comprehensive vertical observations to improve our understanding  
672 of the vertical distribution and chemistry of HONO in the PBL.

673

674 *Data availability.* The data used in this study are available from the corresponding author upon request  
675 (mqin@aiofm.ac.cn).

676

677 *Supplement.*

678

679 *Author contributions.* MQ and PX organized the field contributions from the Anhui Institute of Optics and Fine  
680 Mechanics group for the APHH-Beijing project. MQ and JD designed the study. WF and JD built the IBBCEAS  
681 instrument. JD and KT collected the HONO and NO<sub>2</sub> data. YS and CX provided the ancillary data. FM and MQ  
682 analyzed the data. FM wrote the paper and MQ revised it. The contributions of FM and MQ are the same for this  
683 paper.

684

685 *Competing interests.* The authors declare that they have no conflict of interest.

686

687 *Special issue statement.* This article is part of the special issue “In-depth study of air pollution sources and  
688 processes within Beijing and its surrounding region (APHH-Beijing) (ACP/AMT inter-journal SI)”. It is not  
689 associated with a conference.

690

691 *Acknowledgements.* We gratefully acknowledge Bin Ouyang from Cambridge University for providing HONO  
692 measurement data for inter-comparison.

693

694 *Financial support.* This work was supported by the National Natural Science Foundation of China (41875154,  
695 41571130023, 91544104), the National Key R&D Program of China (2017YFC0209400, 2016YFC0208204), and  
696 the Science and Technology Major Special Project of Anhui Province, China (16030801120).

697

698

699

700

701

702

703

704 **References**

- 705 Aliche, B., Platt, U., Stutz, J.: Impact of nitrous acid photolysis on the total hydroxyl radical budget during the  
706 Limitation of Oxidant Production/Pianura Padana Produzione di Ozono study in Milan, J. Geophys. Res., 107,  
707 LOP 9-1-LOP 9-17, <https://doi.org/10.1029/2000jd000075>, 2002.
- 708 Ammann, M., Kalberer, M., Jost, D. T., Tobler, L., Rossler, E., Pignatelli, D., Gaggeler, H. W., and Baltensperger, U.:  
709 Heterogeneous production of nitrous acid on soot in polluted air masses, Nature, 395, 157-160,  
710 <https://doi.org/10.1038/25965>, 1998.
- 711 An, J., Li, Y., Chen, Y., Li, J., Qu, Y., and Tang, Y. J.: Enhancements of major aerosol components due to additional  
712 HONO sources in the North China Plain and implications for visibility and haze, Adv. Atmos. Sci., 30, 57-66,  
713 <https://doi.org/10.1007/s00376-012-2016-9>, 2012.
- 714 Aubin, D. G., and Abbatt, J. P. D.: Interaction of NO<sub>2</sub> with Hydrocarbon Soot: Focus on HONO Yield, Surface  
715 Modification, and Mechanism, J. Phys. Chem. A., 111, 6263-6273, <https://doi.org/10.1021/jp068884h>, 2007.
- 716 Bao, F. X., Li, M., Zhang, Y., Chen, C. C., and Zhao, J. C.: Photochemical Aging of Beijing Urban PM<sub>2.5</sub>: HONO  
717 Production, Environ. Sci. Technol., 52, 6309-6316, <https://doi.org/10.1021/acs.est.8b00538>, 2018.
- 718 Bartolomei, V., Alvarez, E. G., Wittmer, J., Thili, S., Strekowski, R., Temime-Roussel, B., Quivet, E., Wortham, H.,  
719 Zetzsch, C., Kleffmann, J., and Gligorovski, S.: Combustion Processes as a Source of High Levels of Indoor  
720 Hydroxyl Radicals through the Photolysis of Nitrous Acid, Environ. Sci. Technol., 49, 6599-6607,  
721 <https://doi.org/10.1021/acs.est.5b01905>, 2015.
- 722 Bejan, I., Abd-El-Aal, Y., Barnes, I., Benter, T., Bohn, B., Wiesen, P., and Kleffmann, J.: The photolysis of  
723 *ortho*-nitrophenols: a new gas phase source of HONO, Phys. Chem. Chem. Phys., 8, 2028-2035,  
724 <https://doi.org/10.1039/b516590c>, 2006.
- 725 Bond, T. C., Doherty, S. J., Fahey, D. W., Forster, P. M., Berntsen, T., DeAngelo, B. J., Flanner, M. G., Ghan, S.,  
726 Kärcher, B., Koch, D., Kinne, S., Kondo, Y., Quinn, P.K., Sarofim, M.C., Schultz, M.G., Schulz, M., Venkataraman,  
727 C., Zhang, H., Zhang, S., Bellouin, N., Guttikunda, S.K., Hopke, P.K., Jacobson, M.Z., Kaiser, J.W., Klimont, Z.,  
728 Lohmann, U., Schwarz, J.P., Shindell, D., Storelvmo, T., Warren, S.G., and Zender, C.S.: Bounding the role of  
729 black carbon in the climate system: A scientific assessment, J. Geophys. Res. Atmos., 118, 5380-5552,  
730 <https://doi.org/10.1002/jgrd.50171>, 2013.
- 731 Brigante, M., Cazoir, D., D'Anna, B., George, C., and Donaldson, D. J.: Photoenhanced Uptake of NO<sub>2</sub> by Pyrene  
732 Solid Films, J. Phys. Chem. A, 112, 9503-9508, <https://doi.org/10.1021/jp802324g>, 2008.
- 733 Bröske, R., Kleffmann, J., and Wiesen, P.: Heterogeneous conversion of NO<sub>2</sub> on secondary organic aerosol  
734 surfaces: A possible source of nitrous acid (HONO) in the atmosphere?, Atmos. Chem. Phys., 3, 469-474,  
735 <https://doi.org/10.5194/acp-3-469-2003>, 2003.
- 736 Brown, S. S., Dubé, W. P., Osthoff, H. D., Wolfe, D. E., Angevine, W. M., and Ravishankara, A. R.: High  
737 resolution vertical distributions of NO<sub>3</sub> and N<sub>2</sub>O<sub>5</sub> through the nocturnal boundary layer, Atmos. Chem. Phys., 7,  
738 139-149, <https://doi.org/10.5194/acp-7-139-2007>, 2007.
- 739 Cai, R. L., Yang, D. S., Fu, Y. Y., Wang, X., Li, X. X., Ma, Y., Hao, J. M., Zheng, J., and Jiang, J. K.: Aerosol  
740 surface area concentration: a governing factor in new particle formation in Beijing, Atmos. Chem. Phys., 17,  
741 12327-12340, <https://doi.org/10.5194/acp-17-12327-2017>, 2017.
- 742 Coe, H., and Gallagher, M. W.: Measurements of Dry Deposition of NO<sub>2</sub> to A Dutch Heathland Using the  
743 Eddy-Correlation Technique, Q. J. Roy. Meteor. Soc., 118, 767-786, <https://doi.org/10.1002/qj.49711850608>, 1992.
- 744 Cui, L. L., Li, R., Zhang, Y. C., Meng, Y., Fu, H. B. and Chen, J. M.: An observational study of nitrous acid  
745 (HONO) in Shanghai, China: The aerosol impact on HONO formation during the haze episodes, Sci. Total  
746 Environ., 630, 1057-1070, <https://doi.org/10.1016/j.scitotenv.2018.02.063>, 2018.
- 747 Donaldson, M. A., Berke, A. E., and Raff, J. D.: Uptake of Gas Phase Nitrous Acid onto Boundary Layer Soil

748 Surfaces, *Environ. Sci. Technol.*, 48, 375-383, <https://doi.org/10.1021/es404156a>, 2014.

749 Du, W., Zhao, J., Wang, Y. J., Zhang, Y. J., Wang, Q. Q., Xu, W. Q., Chen, C., Han, T. T., Zhang, F., Li, Z. Q., Fu, P.  
750 Q., Li, J., Wang, Z. F., and Sun, Y. L.: Simultaneous measurements of particle number size distributions at ground  
751 level and 260 m on a meteorological tower in urban Beijing, China, *Atmos. Chem. Phys.*, 17, 6797-6811,  
752 <https://doi.org/10.5194/acp-17-6797-2017>, 2017.

753 Duan, J., Qin, M., Ouyang, B., Fang, W., Li, X., Lu, K. D., Tang, K., Liang, S. X., Meng, F. H., Hu, Z. K., Xie, P.  
754 H., Liu, W. Q., and Häsler, R.: Development of an incoherent broadband cavity-enhanced absorption spectrometer  
755 for in situ measurements of HONO and NO<sub>2</sub>, *Atmos. Meas. Tech.*, 11, 4531-4543,  
756 <https://doi.org/10.5194/amt-11-4531-2018>, 2018.

757 Finlayson-Pitts, B. J., Wingen, L. M., Sumner, A. L., Syomin, D., and Ramazan, K. A.: The heterogeneous  
758 hydrolysis of NO<sub>2</sub> in laboratory systems and in outdoor and indoor atmospheres: An integrated mechanism, *Phys.*  
759 *Chem. Chem. Phys.*, 5, 223-242, <https://doi.org/10.1039/b208564j>, 2003.

760 Finlayson-Pitts, B. J.: Reactions at surfaces in the atmosphere: integration of experiments and theory as necessary  
761 (but not necessarily sufficient) for predicting the physical chemistry of aerosols, *Phys. Chem. Chem. Phys.*, 36,  
762 7760-7779, <https://doi.org/10.1039/B906540G>, 2009.

763 George, C., Strekowski, R. S., Kleffmann, J., Stemmler, K., and Ammann, M.: Photoenhanced uptake of gaseous  
764 NO<sub>2</sub> on solid organic compounds: a photochemical source of HONO?, *Faraday Discuss.*, 130, 195-210,  
765 <https://doi.org/10.1039/b417888m>, 2005.

766 Gómez Alvarez, E., Sörgel, M., Gligorovski, S., Bassil, S., Bartolomei, V., Coulomb, B., Zetzsch, C., and Wortham,  
767 H.: Light-induced nitrous acid (HONO) production from NO<sub>2</sub> heterogeneous reactions on household chemicals,  
768 *Atmos. Environ.*, 95, 391-399, <https://doi.org/10.1016/j.atmosenv.2014.06.034>, 2014.

769 Han, C., Yang, W. J., Wu, Q. Q., Yang, H., and Xue, X. X.: Heterogeneous Photochemical Conversion of NO<sub>2</sub> to  
770 HONO on the Humic Acid Surface under Simulated Sunlight, *Environ. Sci. Technol.*, 50, 5017-5023,  
771 <https://doi.org/10.1021/acs.est.5b05101>, 2016.

772 Han, C., Yang, W. J., Yang, H., and Xue, X. X.: Enhanced photochemical conversion of NO<sub>2</sub> to HONO on humic  
773 acids in the presence of benzophenone, *Environ. Pollut.*, 231, 979-986,  
774 <https://doi.org/10.1016/j.envpol.2017.08.107>, 2017.

775 Hanst, P. L., Spence, J. W., and Miller, M.: Atmospheric Chemistry of N-nitroso Dimethylamine, *Environ. Sci.*  
776 *Technol.*, 11, 403-405, <https://doi.org/10.1021/es60127a007>, 1977.

777 Harrison, R. M., and Kitto, A. M. N.: Evidence for a surface source of atmospheric nitrous acid, *Atmos. Environ.*,  
778 28, 1089-1094, [https://doi.org/10.1016/1352-2310\(94\)90286-0](https://doi.org/10.1016/1352-2310(94)90286-0), 1994.

779 Harrison, R. M., Peak, J. D., and Collins, G. M.: Tropospheric cycle of nitrous acid, *J. Geophys. Res.*, 101,  
780 14429-14439, <https://doi.org/10.1029/96JD00341>, 1996.

781 Hendrick, F., Müller, J. F., Clémer, K., Wang, P., De Mazière, M., Fayt, C., Gielen, C., Hermans, C., Ma, J. Z.,  
782 Pinardi, G., Stavrakou, T., Vlemmix, T., and Van Roozendaal, M.: Four years of ground-based MAX-DOAS  
783 observations of HONO and NO<sub>2</sub> in the Beijing area, *Atmos. Chem. Phys.*, 14, 765-781,  
784 <https://doi.org/10.5194/acp-14-765-2014>, 2014.

785 Hou, S. Q., Tong, S. R., Ge, M. F., and An, J. L.: Comparison of atmospheric nitrous acid during severe haze and  
786 clean periods in Beijing, China, *Atmos. Environ.*, 124, 199-206, <https://doi.org/10.1016/j.atmosenv.2015.06.023>,  
787 2016.

788 Huang, R. J., Yang, L., Cao, J. J., Wang, Q. Y., Tie, X. X., Ho, K. F., Shen, Z. X., Zhang, R. J., Li, G. H., Zhu, C. S.,  
789 Zhang, N. N., Dai, W. T., Zhou, J. M., Liu, S. X., Chen, Y., Chen, J., and O'Dowd, C. D.: Concentration and  
790 sources of atmospheric nitrous acid (HONO) at an urban site in Western China, *Sci. Total Environ.*, 593-594,  
791 165-172, <https://doi.org/10.1016/j.scitotenv.2017.02.166>, 2017.

792 Hao, N., Zhou, B., Chen, D., and Chen, L. M.: Observations of nitrous acid and its relative humidity dependence  
793 in Shanghai, *J. Environ. Sci.*, 18, 910-915, [https://doi.org/10.1016/S1001-0742\(06\)60013-2](https://doi.org/10.1016/S1001-0742(06)60013-2), 2006.

794 Karamchandani, P., Emery, C., Yarwood, G., Lefer, B., Stutz, J., Couzo, E., and Vizuete, W.: Implementation and  
795 refinement of a surface model for heterogeneous HONO formation in a 3-D chemical transport model, *Atmos.*  
796 *Environ.*, 112, 356-368, <https://doi.org/10.1016/j.atmosenv.2015.01.046>, 2015.

797 Kirchstetter, T. W., Harley, R. A., and Littlejohn D.: Measurement of nitrous acid in motor vehicle exhaust,  
798 *Environ. Sci. Technol.*, 30, 2843-2849, <https://doi.org/10.1021/es960135y>, 1996.

799 Kleffmanna, J., Beckera, K. H., and Wiesena, P.: Heterogeneous NO<sub>2</sub> conversion processes on acid surfaces:  
800 possible atmospheric implications, *Atmos. Environ.*, 32, 2721-2729,  
801 [https://doi.org/10.1016/S1352-2310\(98\)00065-X](https://doi.org/10.1016/S1352-2310(98)00065-X), 1998.

802 Kleffmann, J., Becker, K. H., Lackhoff, M., and Wiesen, P.: Heterogeneous conversion of NO<sub>2</sub> on carbonaceous  
803 surfaces, *Phys. Chem. Chem. Phys.*, 1, 5443-5450, <https://doi.org/10.1039/A905545B>, 1999.

804 Kleffmann, J., Kurtenbach, R., Lörzer, J., Wiesen, P., Kalthoff, N., Vogel, B., and Vogel, H.: Measured and  
805 simulated vertical profiles of nitrous acid—Part I: Field measurements, *Atmos. Environ.*, 37, 2949-2955,  
806 [https://doi.org/10.1016/s1352-2310\(03\)00242-5](https://doi.org/10.1016/s1352-2310(03)00242-5), 2003.

807 Kleffmann, J.: Daytime Sources of Nitrous acid (HONO) in the Atmospheric Boundary Layer, *Chemphyschem*, 8,  
808 1137-1144, <https://doi.org/10.1002/cphc.200700016>, 2007.

809 Kurtenbach, R., Becker, K. H., Gomes, J. A. G., Kleffmann, J., Lörzer, J., Spittler, M., Wiesen, P., Ackermann, R.,  
810 Geyer, A., and Platt, U.: Investigations of emission and heterogeneous formation of HONO in a road traffic tunnel,  
811 *Atmos. Environ.*, 35, 3385–3394, [https://doi.org/10.1016/S1352-2310\(01\)00138-8](https://doi.org/10.1016/S1352-2310(01)00138-8), 2001.

812 Laufs, S., Cazaunau, M., Stella, P., Kurtenbach, R., Cellier, P., Mellouki, A., Loubet, B., and Kleffmann, J.: Diurnal  
813 fluxes of HONO above a crop rotation, *Atmos. Chem. Phys.*, 17, 6907-6923,  
814 <https://doi.org/10.5194/acp-17-6907-2017>, 2017.

815 Li, D. D., Xue, L. K., Wen, L., Wang, X. F., Chen, T. S., Mellouki, A., Chen, J. M., and Wang, W. X.:  
816 Characteristics and sources of nitrous acid in an urban atmosphere of northern China: Results from 1-yr continuous  
817 observations, *Atmos. Environ.*, 182, 296-306, <https://doi.org/10.1016/j.atmosenv.2018.03.033>, 2018.

818 Li, S. P., Matthews, J., and Sinha, A.: Atmospheric Hydroxyl Radical Production from Electronically Excited NO<sub>2</sub>  
819 and H<sub>2</sub>O, *Science*, 319, 1657-1660, <https://doi.org/10.1126/science.1151443>, 2008.

820 Li, X., Brauers, T., Häsel, R., Bohn, B., Fuchs, H., Hofzumahaus, A., Holland, F., Lou, S., Lu, K. D., Rohrer, F.,  
821 Hu, M., Zeng, L. M., Zhang, Y. H., Garland, R. M., Su, H., Nowak, A., Wiedensohler, A., Takegawa, N., Shao, M.,  
822 and Wahner, A.: Exploring the atmospheric chemistry of nitrous acid (HONO) at a rural site in Southern China,  
823 *Atmos. Chem. Phys.*, 12, 1497-1513, <https://doi.org/10.5194/acp-12-1497-2012>, 2012.

824 Li, X., Rohrer, F., Hofzumahaus, A., Brauers, T., Häsel, R., Bohn, B., Broch, S., Fuchs, H., Gomm, H., Holland,  
825 F., Jäger, J., Kaiser, J., Keutsch, F. N., Lohse, I., Lu, K. D., Tillmann, R., Wegener, R., Wolfe, G. M., Mentel, T. F.,  
826 Kiendler-Scharr, A., Wahner, A.: Missing Gas-Phase Source of HONO Inferred from Zeppelin Measurement in the  
827 Troposphere, *Science*, 334, 292-296, <https://doi.org/10.1126/science.1248999>, 2014.

828 Liang, Y. T., Zha, Q. Z., Wang, W. H., Cui, L., Lui, K. H., Ho, K. F., Wang, Z., Lee, S. C., and Wang, T.: Revisiting  
829 nitrous acid (HONO) emission from on-road vehicles: A tunnel study with a mixed fleet, *J. Air Waste Manag.*, 67,  
830 797-805, <https://doi.org/10.1080/10962247.2017.1293573>, 2017.

831 Liu, X., Cheng, Y., Zhang, Y., Jung, J., Sugimoto, N., Chang, S.Y., Kim, Y. J., Fan, S., and Zeng, L.: Influences of  
832 relative humidity and particle chemical composition on aerosol scattering properties during the 2006 PRD  
833 campaign, *Atmos. Environ.*, 42, 1525–1536, <https://doi.org/10.1016/j.atmosenv.2007.10.077>, 2008.

834 Liu, Y. H., Lu, K. D., Li, X., Dong, H. B., Tan, Z. F., Wang, H. C., Zou, Q., Wu, Y. S., Zeng, L. M., Hu, M., Min, K.  
835 E., Kecorius, S., Wiedensohler, A., and Zhang, Y. H.: A Comprehensive Model Test of the HONO Sources

836 Constrained to Field Measurements at Rural North China Plain, *Environ. Sci. Technol.*, 53, 3517-3525,  
837 <https://doi.org/10.1021/acs.est.8b06367>, 2019.

838 Liu, Y. L., Nie, W., Xu, Z., Wang, T. Y., Wang, R. X., Li, Y. Y., Wang, L., Chi, X. G., and Ding, A. J.:  
839 Semi-quantitative understanding of source contribution to nitrous acid (HONO) based on 1 year of continuous  
840 observation at the SORPES station in eastern China, *Atmos. Chem. Phys.*, 19, 13289-13308,  
841 <https://doi.org/10.5194/acp-19-13289-2019>, 2019.

842 Liu, Z., Wang, Y. h., Costabile, F., Amoroso, A., Zhao, C., Huey, L. G., Stickel, R., Liao, J., and Zhu, T.: Evidence  
843 of Aerosols as a Media for Rapid Daytime HONO Production over China, *Environ. Sci. Technol.*, 48, 14386-14391,  
844 <https://doi.org/10.1021/es504163z>, 2014.

845 Liu, Z., Wang, Y., Gu, D., Zhao, C., Huey, L. G., Stickel, R., Liao, J., Shao, M., Zhu, T., Zeng, L., Amoroso, A.,  
846 Costabile, F., Chang, C.-C., and Liu, S.-C.: Summertime photochemistry during CAREBeijing-2007:RO<sub>x</sub> budgets  
847 and O<sub>3</sub> formation, *Atmos. Chem. Phys.*, 12, 7737-7752, <https://doi.org/10.5194/acp-12-7737-2012>, 2012.

848 Lu, K. D., Rohrer, F., Holland, F., Fuchs, H., Bohn, B., Brauers, T., Chang, C. C., Häseler, R., Hu, M., Kita, K.,  
849 Kondo, Y., Li, X., Lou, S. R., Nehr, S., Shao, M., Zeng, L. M., Wahner, A., Zhang, Y. H., and Hofzumahaus, A.:  
850 Observation and modelling of OH and HO<sub>2</sub> concentrations in the Pearl River Delta 2006: a missing OH source in a  
851 VOC rich atmosphere, *Atmos. Chem. Phys.*, 12, 1541-1569, <https://doi.org/10.5194/acp-12-1541-2012>, 2012.

852 Ma, Q. X., Wang, T., Liu, C., He, H., Wang, Z., Wang, W. H., and Liang, Y. T.: SO<sub>2</sub> Initiates the Efficient  
853 Conversion of NO<sub>2</sub> to HONO on MgO Surface, *Environ. Sci. Technol.*, 51, 3767-3775,  
854 <https://doi.org/10.1021/acs.est.6b05724>, 2017.

855 Mendez, M., Blond, N., Amedro, D., Hauglustaine, D. A., Blondeau, P., Afif, C., Fittschen, C., and Schoemaeker,  
856 C.: Assessment of indoor HONO formation mechanisms based on in situ measurements and modeling, *Indoor Air*,  
857 27, 443-451, <https://doi.org/10.1111/ina.12320>, 2017.

858 Michoud, V., Colomb, A., Borbon, A., Miet, K., Beekmann, M., Camredon, M., Aumont, B., Perrier, S., Zapf, P.,  
859 Siour, G., Ait-Helal, W., Afif, C., Kukui, A., Furger, M., Dupont, J. C., Haeffelin, M., and Doussin, J. F.: Study of  
860 the unknown HONO daytime source at a European suburban site during the MEGAPOLI summer and winter field  
861 campaigns, *Atmos. Chem. Phys.*, 14, 2805-2822, <https://doi.org/10.5194/acp-14-2805-2014>, 2014.

862 Michoud, V., Doussin, J.-F., Colomb, A., Afif, C., Borbon, A., Camredon, M., Aumont, B., Legrand, M., and  
863 Beekmann, M.: Strong HONO formation in a suburban site during snowy days, *Atmos. Environ.*, 116, 155-158,  
864 <https://doi.org/10.1016/j.atmosenv.2015.06.040>, 2015.

865 Monge, M. E., D'Anna, B., Mazri, L., Giroir-Fendler, A., Ammann, M., Donaldson, D. J., and George, C.: Light  
866 changes the atmospheric reactivity of soot, *P. Natl. Acad. Sci. USA*, 107, 6605-6609,  
867 <https://doi.org/10.1073/pnas.0908341107>, 2010.

868 Oswald, R., Behrendt, T., Ermel, M., Wu, D., Su, H., Cheng, Y., Breuninger, C., Moravek, A., Mouglin, E., Delon,  
869 C., Loubet, B., Pommerening-Röser, A., Sörgel, M., Pöschl, U., Hoffmann, T., Andreae, M. O., Meixner, F. X. and  
870 Trebs, I.: HONO Emissions from Soil Bacteria as a Major source of Atmospheric Reactive Nitrogen, *Science*, 341,  
871 1233-1235, <https://doi.org/10.1126/science.1242266>, 2013.

872 Oswald, R., Ermel, M., Hens, K., Novelli, A., Ouwersloot, H. G., Paasonen, P., Petäjä, T., Sipilä, M., Keronen, P.,  
873 Bäck, J., Königstedt, R., Hosaynali Beygi, Z., Fischer, H., Bohn, B., Kubistin, D., Harder, H., Martinez, M.,  
874 Williams, J., Hoffmann, T., Trebs, I., and Sörgel, M.: A comparison of HONO budgets for two measurement  
875 heights at a field station within the boreal forest in Finland, *Atmos. Chem. Phys.*, 15, 799-813,  
876 <https://doi.org/10.5194/acp-15-799-2015>, 2015.

877 Pitts, J. N., Grosjean, D., Cauwenberghe, K. V., Schmid, J. P., and Fitz, D. R.: Photooxidation of aliphatic amines  
878 under simulated atmospheric conditions: formation of nitrosamines, nitramines, amides, and photochemical  
879 oxidant, *Environ. Sci. Technol.*, 12, 946-953, <https://doi.org/10.1021/es60144a009>, 1978.

880 Rappenglück, B., Lubertino, G., Alvarez, S., Golovko, J., Czader, B., and Ackermann, L.: Radical precursors and  
881 related species from traffic as observed and modeled at an urban highway junction, *J. Air Waste Manag. Assoc.*, 63,  
882 1270-1286, <https://doi.org/10.1080/10962247.2013.822438>, 2013.

883 Reisinger, A. R.: Observations of HNO<sub>2</sub> in the polluted winter atmosphere: possible heterogeneous production on  
884 aerosols, *Atmos. Environ.*, 34, 3865-3874, [https://doi.org/10.1016/S1352-2310\(00\)00179-5](https://doi.org/10.1016/S1352-2310(00)00179-5), 2000.

885 Saastad, O. W., Ellermann, T., and Nielsen, C., J.: On the adsorption of NO and NO<sub>2</sub> on cold H<sub>2</sub>O/H<sub>2</sub>SO<sub>4</sub> surfaces,  
886 *Geophys. Res. Lett.*, 20, 1191-1193, <https://doi.org/10.1029/93GL01621>, 1993.

887 Scharko, N. K., Martin, E. T., Losovj, Y., Peters, D. G., and Raff, J. D.: Evidence for Quinone Redox Chemistry  
888 Mediating Daytime and Nighttime NO<sub>2</sub>-to-HONO Conversion on Soil Surfaces, *Environ. Sci. Technol.*, 51,  
889 9633-9643, <https://doi.org/10.1021/acs.est.7b01363>, 2017.

890 Sleiman, M., Gundel, L. A., Pankow, J. F., Jacob III, P., Singer, B. C., and Destailhats, H.: Formation of  
891 carcinogens indoors by surface-mediated reactions of nicotine with nitrous acid, leading to potential thirdhand  
892 smoke hazards, *P. Natl. Acad. Sci. USA*, 107, 6576-6581, <https://doi.org/10.1073/pnas.0912820107>, 2010.

893 Sörgel, M., Regelin, E., Bozem, H., Diesch, J. M., Drewnick, F., Fischer, H., Harder, H., Held, A.,  
894 Hosaynali-Beygi, Z., Martinez, M., and Zetzsch, C.: Quantification of the unknown HONO daytime source and its  
895 relation to NO<sub>2</sub>, *Atmos. Chem. Phys.*, 11, 10433-10447, <https://doi.org/10.5194/acp-11-10433-2011>, 2011.

896 Spataro, F., Ianniello, A., Esposito, G., Allegrini, I., Zhu, T., and Hu, M.: Occurrence of atmospheric nitrous acid in  
897 the urban area of Beijing (China), *Sci. Total Environ.*, 447, 210-224,  
898 <https://doi.org/10.1016/j.scitotenv.2012.12.065>, 2013.

899 Spindler, G., Brüggemann, E., and Herrmann, H.: Nitrous acid (HNO<sub>2</sub>) Concentration Measurements and  
900 Estimation of Dry Deposition over Grassland in Eastern Germany, *Transactions on Ecology and Environment*, 28,  
901 223-227, 1999.

902 Stemmler, K., Ammann, M., Donders, C., Kleffmann, J., and George, C.: Photosensitized reduction of nitrogen  
903 dioxide on humic acid as a source of nitrous acid, *Nature*, 440, 195-198, <https://doi.org/10.1038/nature04603>,  
904 2006.

905 Stutz, J., Alicke, B., Neftel, A.: Nitrous acid formation in the urban atmosphere: Gradient measurements of NO<sub>2</sub>  
906 and HONO over grass in Milan, Italy, *J. Geophys. Res.*, 107, LOP 5-1-LOP 5-15,  
907 <https://doi.org/10.1029/2001JD000390>, 2002.

908 Stutz, J., Alicke, B., Ackermann, R., Geyer, A., Wang, S. H., White, A. B., Williams, E. J., Spicer, C. W., and Fast,  
909 J. D.: Relative humidity dependence of HONO chemistry in urban areas, *J. Geophys. Res.-Atmos.*, 109, D03307,  
910 <https://doi.org/10.1029/2003JD004135>, 2004a.

911 Stutz, J., Alicke, B., Ackermann, R., Geyer, A., White, A., and Williams, E.: Vertical profiles of NO<sub>3</sub>, N<sub>2</sub>O<sub>5</sub>, O<sub>3</sub>,  
912 and NO<sub>x</sub> in the nocturnal boundary layer: 1. Observations during the Texas Air Quality Study 2000, *J. Geophys. Res.-Atmos.*, 109, D12306, <https://doi.org/10.1029/2003JD004209>, 2004b.

914 Su, H., Cheng, Y. F., Cheng, P., Zhang, Y. H., Dong, S. F., Zeng, L. M., Wang, X. S., Slanina, J., Shao, M., and  
915 Wiedensohler, A.: Observation of nighttime nitrous acid (HONO) formation at a non-urban site during  
916 PRIDE-PRD2004 in China, *Atmos. Environ.*, 42, 6219-6232, <https://doi.org/10.1016/j.atmosenv.2008.04.006>,  
917 2008a.

918 Su, H., Cheng, Y. F., Shao, M., Gao, D. F., Yu, Z. Y., Zeng, L. M., Slanina, J., Zhang, Y. H., and Wiedensohler, A.:  
919 Nitrous acid (HONO) and its daytime sources at a rural site during the 2004 PRIDE-PRD experiment in China, *J.*  
920 *Geophys. Res.*, 113, D14312, <https://doi.org/10.1029/2007JD009060>, 2008b.

921 Su, H., Cheng, Y. F., Oswald, R., Behrendt, T., Trebs, I., Meixner, F. X., Andreae, M. O., Cheng, P., Zhang, Y. H.,  
922 and Pöschl, U.: Soil nitrite as a Source of Atmospheric HONO and OH Radicals, *Science*, 333, 1616-1618,  
923 <https://doi.org/10.1126/science.1207687>, 2011.



924 Sun, Y. L., Wang, Z. F., Fu, P. Q., Yang, T., Jiang, Q., Dong, H. B., Li, J., and Jia, J. J.: Aerosol composition,  
925 sources and processes during wintertime in Beijing, China, *Atmos. Chem. Phys.*, 13, 4577-4592,  
926 <https://doi.org/10.5194/acp-13-4577-2013>, 2013.

927 Sun, Y. L., Jiang, Q., Wang, Z. F., Fu, P. Q., Li, J., Yang, T., and Yin, Y.: Investigation of the sources and evolution  
928 processes of severe haze pollution in Beijing in January 2013, *J. Geophys. Res. Atmos.*, 119, 4380-4398,  
929 <https://doi.org/10.1002/2014JD021641>, 2014.

930 Tan, Z. F., Fuchs, H., Lu, K. D., Hofzumahaus, A., Bohn, B., Broch, S., Dong, H. B., Gomm, S., Häsel, R., He, L.  
931 Y., Holland, F., Li, X., Liu, Y., Lu, S. H., Rohrer, F., Shao, M., Wang, B. L., Wang, M., Wu, Y. S., Zeng, L. M.,  
932 Zhang, Y. S., Wahner, A., and Zhang, Y. H.: Radical chemistry at a rural site (Wangdu) in the North China Plain:  
933 observation and model calculations of OH, HO<sub>2</sub> and RO<sub>2</sub> radicals, *Atmos. Chem. Phys.*, 17, 663-690,  
934 <https://doi.org/10.5194/acp-17-663-2017>, 2017.

935 Tang, K., Qin, M., Duan, J., Fang, W., Meng, F. H., Liang, S. X., Xie, P. H., Liu, J. G., Liu, W. Q., Xue, C. Y., and  
936 Mu, Y. J.: A dual dynamic chamber system based on IBBCEAS for measuring fluxes of nitrous acid in agricultural  
937 fields in the North China Plain, *Atmos. Environ.*, 196, 10-19, <https://doi.org/10.1016/j.atmosenv.2018.09.059>,  
938 2019.

939 Tang, Y., An, J., Wang, F., Li, Y., Qu, Y., Chen, Y., and Lin, J.: Impacts of an unknown daytime HONO source on  
940 the mixing ratio and budget of HONO, and hydroxyl, hydroperoxyl, and organic peroxy radicals, in the coastal  
941 regions of China, *Atmos. Chem. Phys.*, 15, 9381-9398, <https://doi.org/10.5194/acp-15-9381-2015>, 2015.

942 Tong, S. R., Hou, S. Q., Zhang, Y., Chu, B. W., Liu, Y. C., He, H., Zhao, P. S., and Ge, M. F.: Exploring the nitrous  
943 acid (HONO) formation mechanism in winter Beijing: direct emissions and heterogeneous production in urban and  
944 suburban areas, *Faraday Discuss.*, 189, 213-230, <https://doi.org/10.1039/c5fd00163c>, 2016.

945 Trinh, H. T., Imanishi, K., Morikawa, T., Hagino, H., and Takenaka N.: Gaseous nitrous acid (HONO) and nitrogen  
946 oxides (NO<sub>x</sub>) emission from gasoline and diesel vehicles under real-world driving test cycles, *J. Air Waste Manage.*  
947 *Assoc.*, 67, 412-420, <https://doi.org/10.1080/10962247.2016.1240726>, 2017.

948 VandenBoer, T. C., Brown, S. S., Murphy, J. G., Keene, W. C., Young, C. J., Pszenny, A. A. P., Kim, S., Warneke,  
949 C., de Gouw, J. A., Maben, J. R., Wagner, N. L., Riedel, T. P., Thornton, J. A., Wolfe, D. E., Dubé, W. P., Öztürk, F.,  
950 Brock, C. A., Grossberg, N., Lefer, B., Lerner, B., Middlebrook, A. M., and Roberts, J. M.: Understanding the role  
951 of the ground surface in HONO vertical structure: High resolution vertical profiles during NACHTT-11, *J. Geophys.*  
952 *Res.- Atmos.*, 118, 10155-110171, <https://doi.org/10.1002/jgrd.50721>, 2013.

953 Villena, G., Kleffmann, J., Kurtenbach, R., Wiesen, P., Lissi, E., Rubio, M. A., Croxatto, G., and Rappenglück, B.:  
954 Vertical gradients of HONO, NO<sub>x</sub> and O<sub>3</sub> in Santiago de Chile, *Atmos. Environ.*, 45, 3867-3873,  
955 <https://doi.org/10.1016/j.atmosenv.2011.01.073>, 2011.

956 Vogel, B., Vogel H., Kleffmann, J., and Kurtenbach, R.: Measured and simulated vertical profiles of nitrous  
957 acid—Part II. Model simulations and indications for a photolytic source, *Atmos. Environ.*, 37, 2957-2966,  
958 [https://doi.org/10.1016/S1352-2310\(03\)00243-7](https://doi.org/10.1016/S1352-2310(03)00243-7), 2003.

959 Wang, H. C., Lu, K. D., Chen, X. R., Zhu, Q. D., Wu, Z. J., Wu, Y. S., and Sun, K.: Fast particulate nitrate  
960 formation via N<sub>2</sub>O<sub>5</sub> uptake aloft in winter in Beijing, *Atmos. Chem. Phys.*, 18, 10483-10495,  
961 <https://doi.org/10.5194/acp-18-10483-2018>, 2018.

962 Wang, J. Q., Zhang, X. S., Guo, J., Wang, Z. W., and Zhang, M. G.: Observation of nitrous acid (HONO) in Beijing,  
963 China: Seasonal variation, nocturnal formation and daytime budget, *Sci. Total Environ.*, 587-588, 350-359,  
964 <https://doi.org/10.1016/j.scitotenv.2017.02.159>, 2017.

965 Wang, S. S., Zhou, R., Zhao, H., Wang, Z. R., Chen, L. M., and Zhou, B.: Long-term observation of atmospheric  
966 nitrous acid (HONO) and its implication to local NO<sub>2</sub> levels in Shanghai, China, *Atmos. Environ.*, 77, 718-724,  
967 <https://doi.org/10.1016/j.atmosenv.2013.05.071>, 2013.

968 Wong, K. W., Oh, H. -J., Lefer, B. L., Rappenglück, B., and Stutz, J.: Vertical profiles of nitrous acid in the  
969 nocturnal urban atmosphere of Houston, TX, *Atmos. Chem. Phys.*, 11, 3595-3609,  
970 <https://doi.org/10.5194/acp-11-3595-2011>, 2011.

971 Wong, K. W., Tsai, C., Lefer, B., Haman, C., Grossberg, N., Brune, W. H., Ren, X., Luke, W., and Stutz, J.:  
972 Daytime HONO vertical gradients during SHARP 2009 in Houston, TX, *Atmos. Chem. Phys.*, 12, 635-652,  
973 <https://doi.org/10.5194/acp-12-635-2012>, 2012.

974 Wong, K. W., Tsai, C., Lefer, B., Grossberg, N., and Stutz, J.: Modeling of daytime HONO vertical gradients  
975 during SHARP 2009, *Atmos. Chem. Phys.*, 13, 3587-3601, <https://doi.org/10.5194/acp-13-3587-2013>, 2013.

976 Xie, C. H., Xu, W. Q., Wang, J. F., Wang, Q. Q., Liu, D. T., Tang, G. Q., Chen, P., Du, W., Zhao, J., Zhang, Y. J.,  
977 Zhou, W., Han, T. T., Bian, Q. Y., Li, J., Fu, P. Q., Wang, Z. F., Ge, X. L., Allan, J., Coe, H., and Sun, Y. L.: Vertical  
978 characterization of aerosol optical properties and brown carbon in winter in urban Beijing, China, *Atmos. Chem.*  
979 *Phys.*, 19, 165–179, <https://doi.org/10.5194/acp-19-165-2019>, 2019.

980 Xu, W. Q., Sun, Y. L., Wang, Q. Q., Zhao, J., Wang, J. F., Ge, X. L., Xie, C. H., Zhou, W., Du, W., Li, J., Fu, P. Q.,  
981 Wang, Z. F., Worsnop, D. R., and Coe, H.: Changes in Aerosol Chemistry From 2014 to 2016 in Winter in Beijing:  
982 Insights From High-Resolution Aerosol Mass Spectrometry, *J. Geophys. Res.- Atmos.*, 124, 1132-1147,  
983 <https://doi.org/10.1029/2018JD029245>, 2019.

984 Xu, Z., Wang, T., Wu, J. Q., Xue, L. K., Chan, J., Zha, Q., Z., Zhou, S. Z., Louie, P. K. K., and Luk, C. W. Y.:  
985 Nitrous acid (HONO) in a polluted subtropical atmosphere: Seasonal variability, direct vehicle emissions and  
986 heterogeneous production at ground surface, *Atmos. Environ.*, 106, 100-109,  
987 <https://doi.org/10.1016/j.atmosenv.2015.01.061>, 2015.

988 Yang, Q., Su, H., Li, X., Cheng, Y. F., Lu, K. D., Cheng, P., Gu, J. W., Guo, S., Hu, M., Zeng, L. M., Zhu, T., and  
989 Zhang, Y. H.: Daytime HONO formation in the suburban area of the megacity Beijing, China, *Sci. China Chem.*,  
990 57, 1032-1042, <https://doi.org/10.1007/s11426-013-5044-0>, 2014.

991 Ye, C. X., Zhang, N., Gao, H. L., and Zhou, X. L.: Photolysis of Particulate Nitrate as a Source of HONO and NO<sub>x</sub>,  
992 *Environ. Sci. Technol.*, 51, 6849-6856, <https://doi.org/10.1021/acs.est.7b00387>, 2017.

993 Ye, C. X., Zhou, X. L., Pu, D., Stutz, J., Festa, J., Spolaor, M., Tsai, C., Cantrell, C., Mauldin III, R. L.,  
994 Weinheimer, A., Hornbrook, R. S., Apel, E. C., Guenther, A., Kaser, L., Yuan, B., Karl, T., Haggerty, J., Hall, S.,  
995 Ullmann, K., Smith, J., and Ortega, J.: Tropospheric HONO distribution and chemistry in the southeastern US,  
996 *Atmos. Chem. Phys.*, 18, 9107-9120, <https://doi.org/10.5194/acp-18-9107-2018>, 2018.

997 Yu, Y., Galle, B., Panday, A., Hodson, E., Prinn, R., and Wang, S.: Observations of high rates of NO<sub>2</sub>-HONO  
998 conversion in the nocturnal atmospheric boundary layer in Kathmandu, Nepal, *Atmos. Chem. Phys.*, 9, 6401-6415,  
999 <https://doi.org/10.5194/acp-9-6401-2009>, 2009.

1000 Zhang, N., Zhou, X. L., Shepson, P. B., Gao, H. L., Alaghmand, M., and Stirm, B.: Aircraft measurement of  
1001 HONO vertical profiles over a forested region, *Geophys. Res. Lett.*, 36, L15820,  
1002 <https://doi.org/10.1029/2009GL038999>, 2009.

1003 Zhang, R., Wang, G., Guo, S., Zamora, M. L., Ying, Q., Lin, Y., Wang, W., Hu, M., and Wang, Y.: Formation of  
1004 Urban Fine Particulate Matter, *Chem. Rev.*, 115, 3303-3855, <https://doi.org/10.1021/acs/chemrev.5b00067>, 2015.

1005 Zhang, W. Q., Tong, S. R., Ge, M. F., An, J. L., Shi, Z. B., Hou, S. Q., Xia, K. H., Qu, Y., Zhang, H. X., Chu, B. W.,  
1006 Sun, Y. L., and He, H.: Variations and sources of nitrous acid (HONO) during a severe pollution episode in Beijing  
1007 in winter 2016, *Sci. Total Environ.*, 648, 253-262, <https://doi.org/10.1016/j.scitotenv.2018.08.133>, 2018.

**Table**

**Table 1.** Classification of the meteorological conditions and corresponding concentrations of NR-PM<sub>1</sub>, NO<sub>2</sub> and HONO from December 7<sup>th</sup> to 12<sup>th</sup>.

Time period	Weather condition	NR-PM <sub>1</sub> (μg·m <sup>-3</sup> )	HONO (ppb)	NO <sub>2</sub> (ppb)	WS (m·s <sup>-1</sup> )	WD	T (°C)	RH (%)
7 Dec–8 Dec (10:00)	Haze (E1)	30–184	1.49–7.59	24.91–65.48	0.03–1.95	NW-ESE <sup>a</sup>	1.6–9.3	36–82
8 Dec (10:00)–11 Dec	Clean (C2)	3–97	0.05–3.75 0.27–3.75	3.33–47.84	0.01–6.24	NE-NW	-2.4–9.1	16–53
11 Dec–12 Dec	Haze (E3)	69–217	1.54–5.51	38.58–66.57	0.02–1.81	NE-NW	-1.6–6.9	40–69

<sup>a</sup> NE: Northeast; ESE: East-southeast; NW: Northwest;

**Table 2.** The nocturnal gradient of HONO and NO<sub>2</sub> throughout the vertical measurements. The linear least squares regression slope and correlation coefficient of HONO and NO<sub>2</sub> to altitude identified in each vertical profile measurement.

Date	Time period (hh:mm, LT)	Gradient-HONO (ppt m <sup>-1</sup> )	R <sup>2</sup>	Gradient-NO <sub>2</sub> (ppt m <sup>-1</sup> )	R <sup>2</sup>
9/12/2016	22:42–23:06	-4.49 ± 0.31	0.90	-14.38 ± 1.62	0.77
9/12/2016	23:15–23:40	-4.35 ± 0.70	0.62	-16.54 ± 1.85	0.77
10/12/2016	22:36–23:01	-1.08 ± 0.49	0.15	-2.97 ± 1.53	0.11
10/12/2016	23:01–23:25	-3.61 ± 0.50	0.60	-7.59 ± 1.24	0.62
11/12/2016	22:35–23:00	-6.91 ± 0.33	0.95	-9.53 ± 1.01	0.79
11/12/2016	23:04–23:29	-0.03 ± 0.43	0.0003	-5.32 ± 0.80	0.67
12/12/2016	00:00–00:26	0.23 ± 0.36	0.02	-5.21 ± 0.79	0.65
12/12/2016	00:45–01:09	-1.79 ± 0.28	0.64	-5.28 ± 0.84	0.63

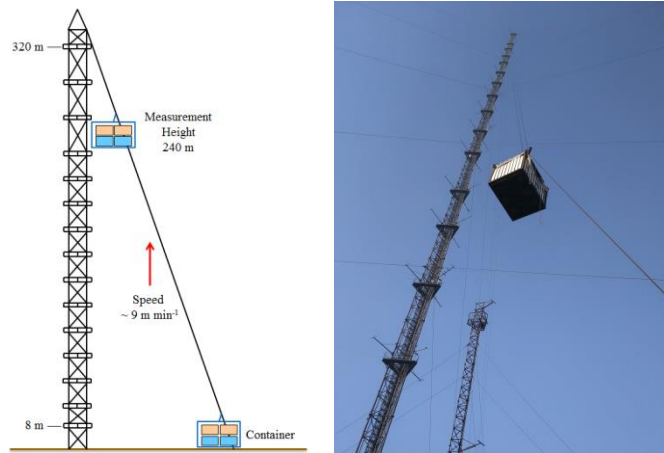
Date	Time period (hh:mm, LT)	Gradient-HONO (ppt m <sup>-1</sup> )	R <sup>2</sup>	Gradient-NO <sub>2</sub> (ppt m <sup>-1</sup> )	R <sup>2</sup>
9/12/2016	22:42–23:06	-4.56 ± 0.34	0.89	-16.41 ± 1.22	0.89
9/12/2016	23:15–23:40	-4.70 ± 0.73	0.65	-18.69 ± 1.50	0.87
10/12/2016	22:36–23:01	-0.45 ± 0.34	0.04	-2.22 ± 1.23	0.10
10/12/2016	23:01–23:25	-3.36 ± 0.52	0.65	-7.59 ± 1.24	0.62

11/12/2016	22:35–23:00	$-6.92 \pm 0.36$	0.94	$-10.52 \pm 0.91$	0.86
11/12/2016	23:04–23:29	$-0.16 \pm 0.46$	0.006	$-5.45 \pm 0.87$	0.63
12/12/2016	00:00–00:26	$0.24 \pm 0.39$	0.02	$-6.01 \pm 0.69$	0.77
12/12/2016	00:45–01:09	$-1.98 \pm 0.28$	0.71	$-5.70 \pm 0.87$	0.65

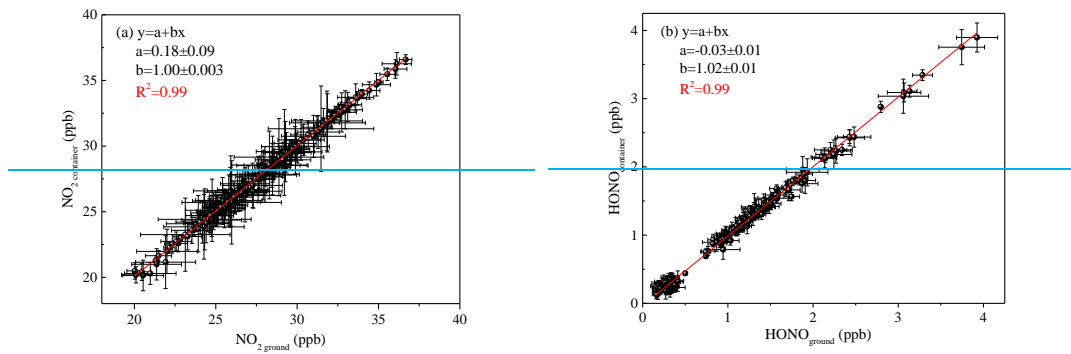
**Table 3.** Emission ratios ( $\Delta\text{HONO}/\Delta\text{NO}_x$ ) of the fresh direct emission plumes.

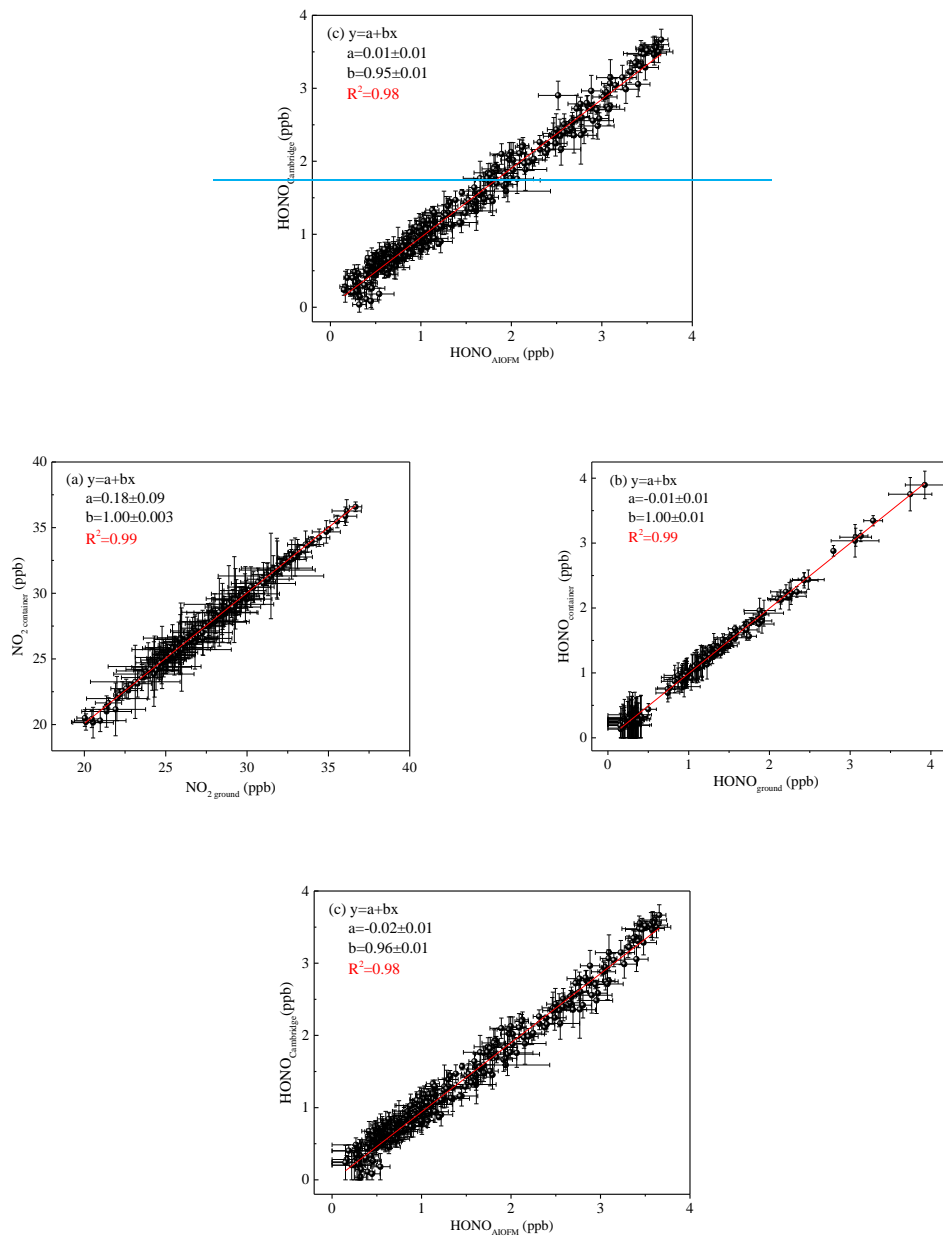
Date	Local Time	R <sup>2</sup>	$\Delta\text{NO}/\Delta\text{NO}_x$	$\Delta\text{HONO}/\Delta\text{NO}_x$ (%)
15/11/2016	18:05–18:15	0.97	0.99	1.07
16/11/2016	20:50–21:10	0.83	0.96	0.92
24/11/2016	20:50–21:10	0.92	1.13	1.12
26/11/2019	02:10–02:40	0.94	0.94	1.31
26/11/2016	22:15–22:30	0.95	1.00	1.73
28/11/2019	04:40–04:55	0.87	0.85	0.78
29/11/2016	03:30–03:50	0.95	0.98	1.60
2/12/2016	23:40–23:55	0.95	1.01	1.67
7/12/2016	02:25–02:35	0.87	0.90	1.67
10/12/2016	01:00–01:25	0.84	0.95	1.43
10/12/2016	02:40–02:55	0.86	0.93	0.79

## Figures

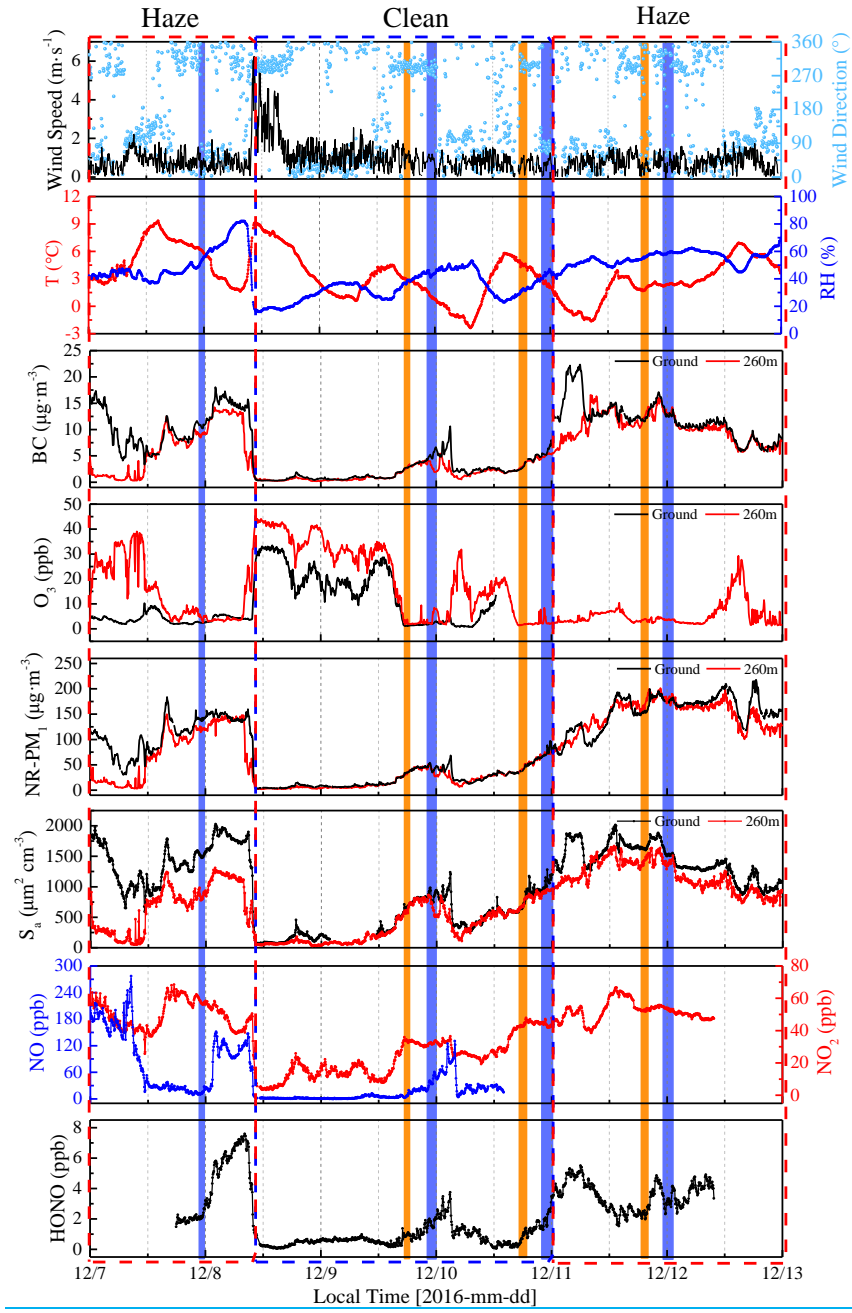


**Figure 1.** The Beijing 325-m meteorological tower (BMT) at the Institute of Atmospheric Physics (IAP).





**Figure 2.** (a) Correlation of  $\text{NO}_2$  concentration was measured using the two IBBCEAS instruments; (b) correlation of HONO concentration was measured using the two IBBCEAS instruments; (c) an inter-comparison between the IBBCEAS of Cambridge University and the IBBCEAS of the Anhui Institute of Optics and Fine Mechanics (AIOFM). The solid lines (red lines) show the orthogonal linear least squares regression between the two IBBCEAS instruments



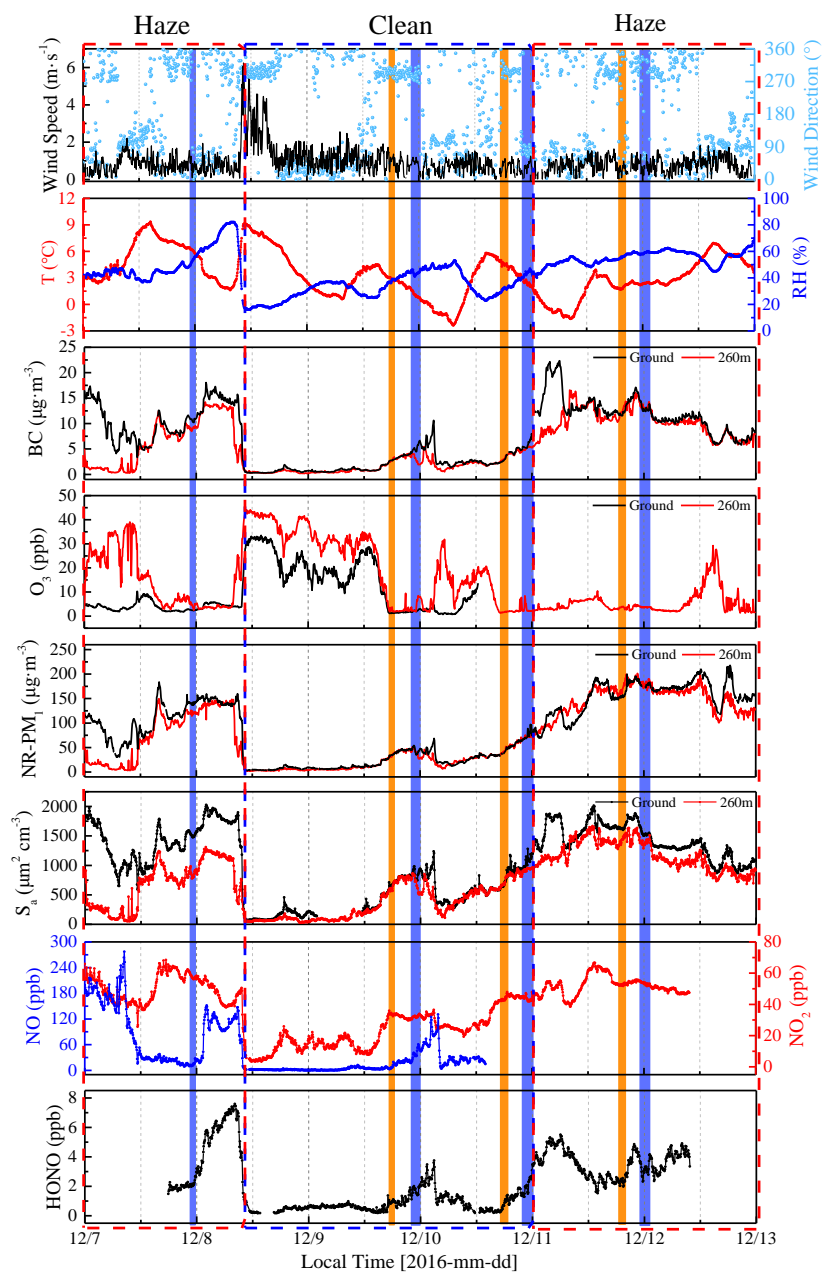


**Figure 3.** Time-series of wind speed (WS) and direction (WD), temperature ( $T$ ), relative humidity (RH), BC,  $O_3$ , NR- $PM_{10}$ , aerosol surface area ( $S_a$ ), NO,  $NO_2$ , and HONO from December 7<sup>th</sup> to 12<sup>th</sup> 2016 at the IAP-Tower Division in Beijing, China. The shaded region represents the eight vertical measurements (Table S1). The orange shaded region represents the vertical measurements after sunset, and the violet shaded region represents the vertical measurements at night and midnight.



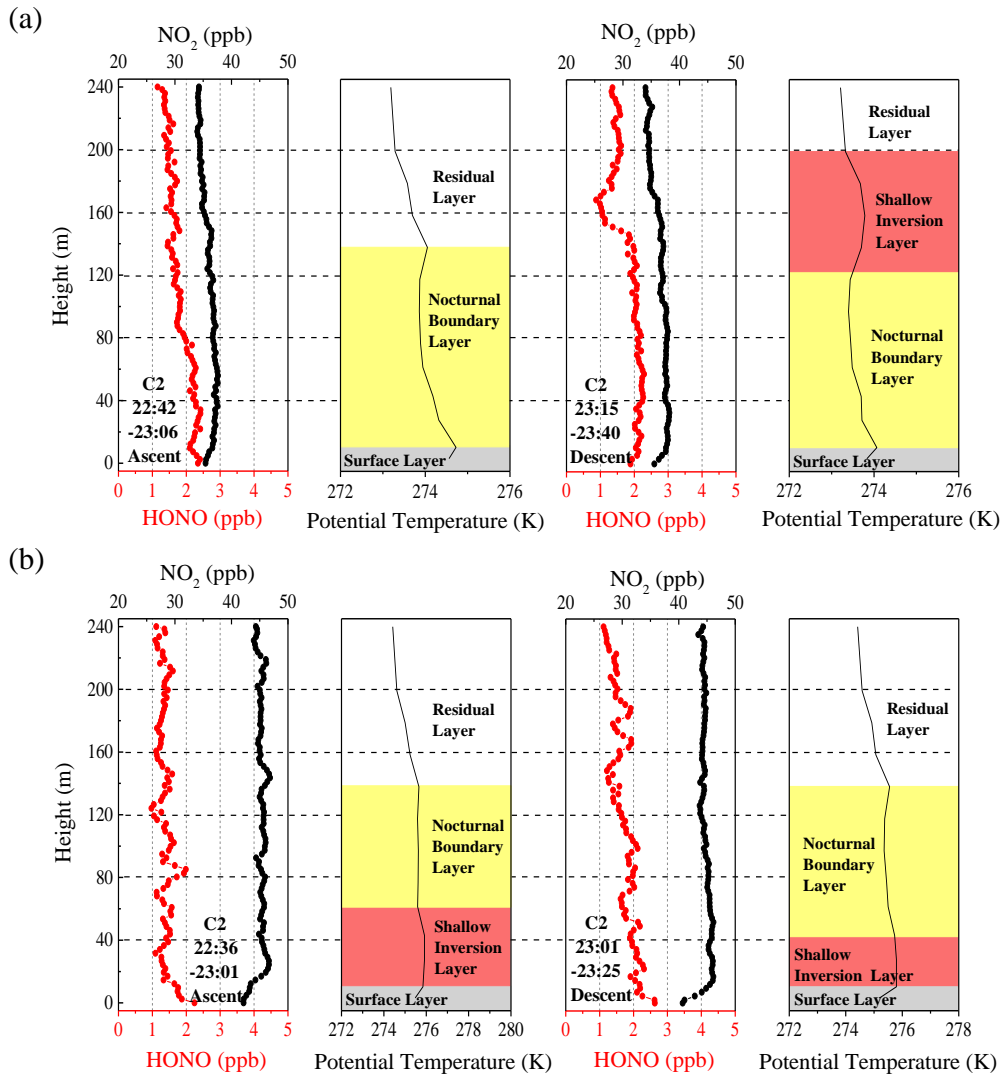


**Figure 4.** Nocturnal vertical profiles of HONO, NO<sub>2</sub>, and the potential temperatures during the ascent and descent of the container on the (a) 9<sup>th</sup> and (b) 10<sup>th</sup> of December. The time in the figure corresponds to the measurement time of the vertical profile of the HONO and NO<sub>2</sub>. The different colored shaded region indicates the nocturnal small-scale stratification (surface layer, nocturnal boundary layer, shallow inversion layer, and residual layer). The heights of the surface layer, the shallow inversion layer, the nocturnal boundary layer, and the residual layer are denoted by grey shaded regions, pink shaded regions, yellow shaded regions, and white shaded regions, respectively.

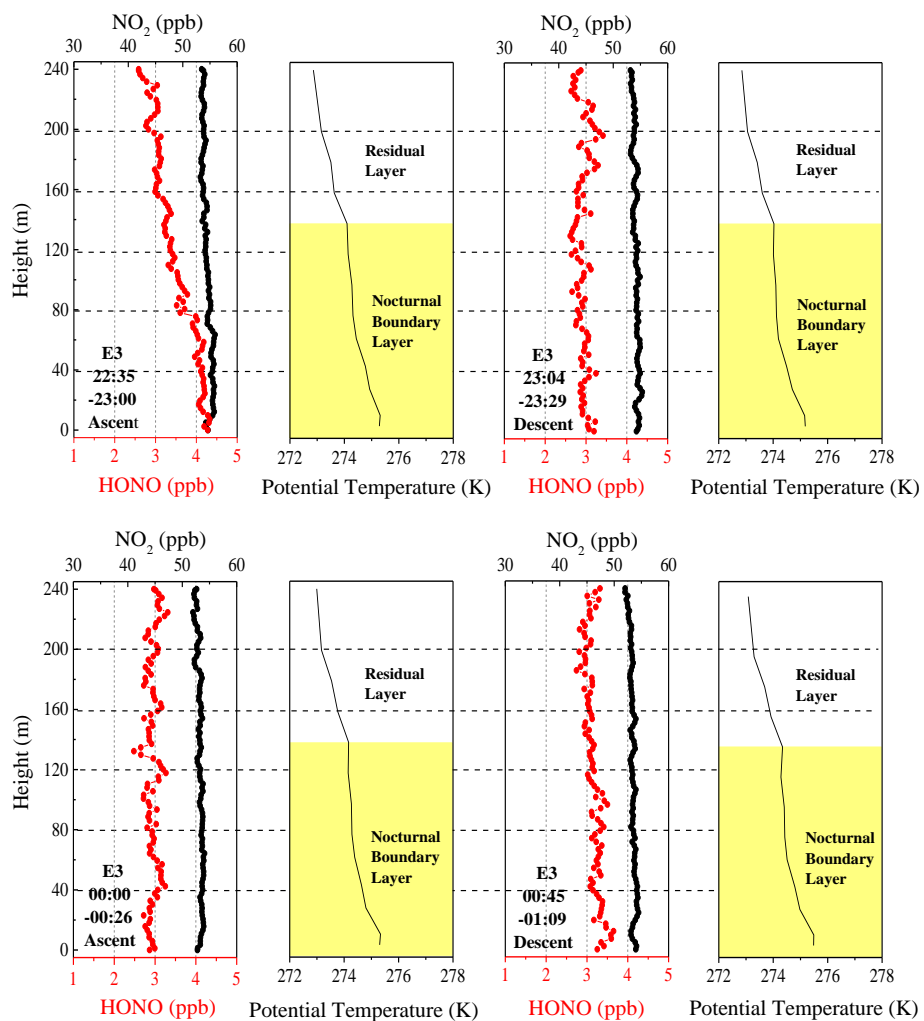


**Figure 5.** Vertical profiles of HONO and NO<sub>2</sub> on the night of December 11<sup>th</sup> and midnight of December 12<sup>th</sup>. The potential temperature profiles indicate nocturnal small-scale stratification (a nocturnal boundary layer and a residual layer). The height of the nocturnal boundary layer (NBL) is denoted by the yellow shaded region. The time in the figure corresponds to the measurement time of the vertical profiles of HONO and NO<sub>2</sub>.

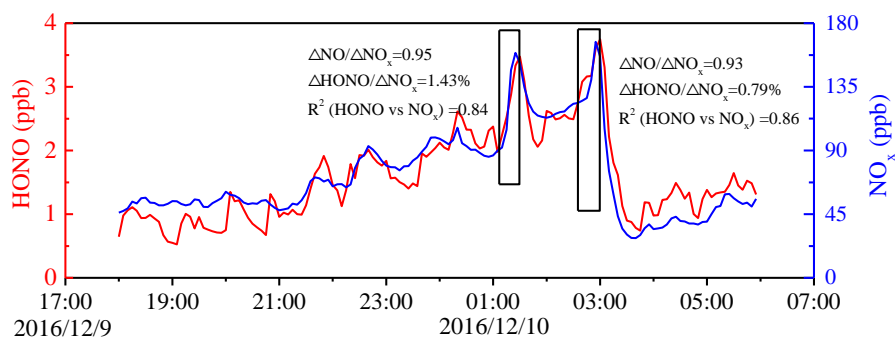


**Figure 6.** Temporal variation of nocturnal HONO and NO<sub>x</sub> on December 9<sup>th</sup> to 10<sup>th</sup>, 2016. The HONO emission ratios were estimated using data collected in the black frame.

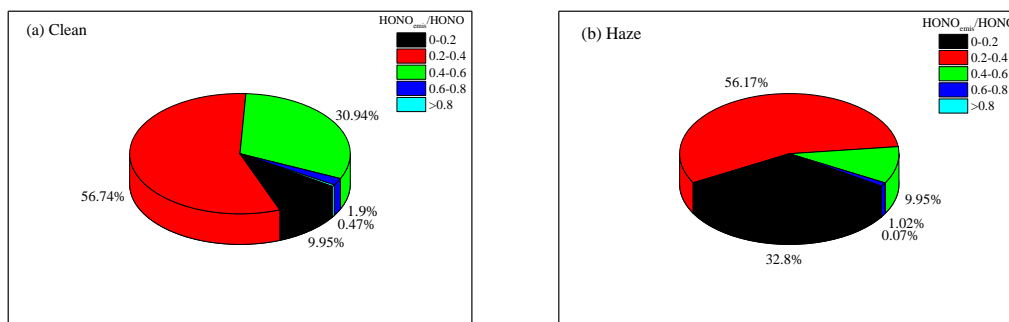


**Figure 7.** The nocturnal HONO<sub>emis</sub>/HONO ratios frequency distribution during (a) clean and (b) haze episodes.

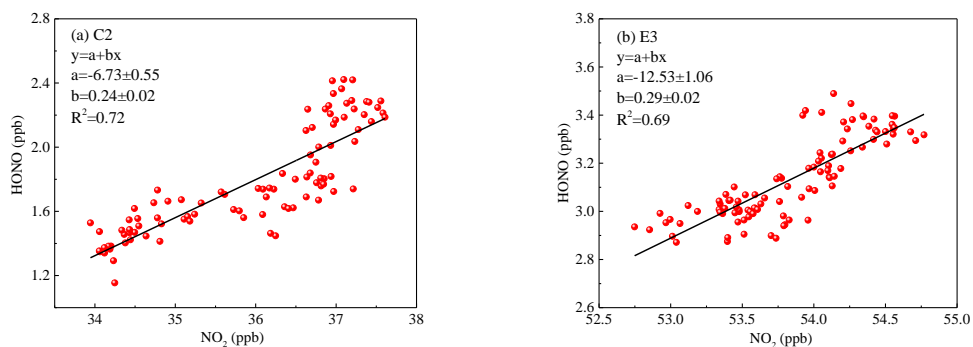


**Figure 8.** The correlation of the vertical profiles between HONO and  $\text{NO}_2$  during (a) the clean episode (C2) and (b) the haze episode (E3) using a linear least squares regression fit.

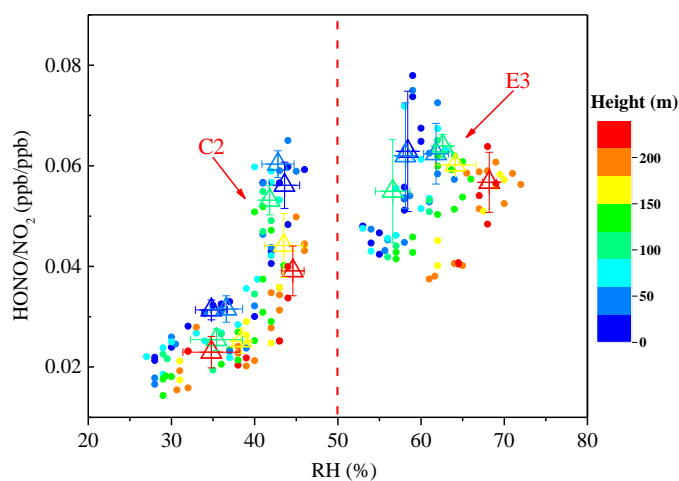


**Figure 9.** Scatter plot of  $\text{HONO}/\text{NO}_2$  against RH of all vertical profiles during the clean episode (C2) and the haze episode (E3). The  $\text{HONO}/\text{NO}_2$  ratio is color coded by the heights. Triangles are the average of the first five  $\text{HONO}/\text{NO}_2$  values in each 10% RH interval at different height intervals (8–65 m, 65–120 m, 120–180 m, and 180–240 m).

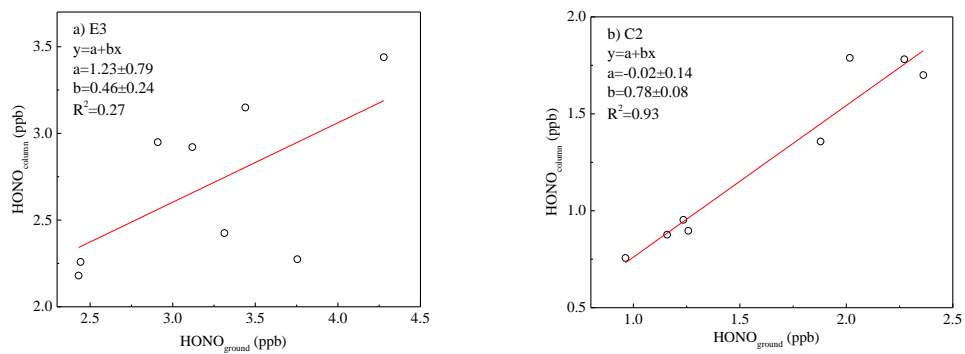


**Figure 10.** Orthogonal linear least squares correlation between the column average concentration of HONO (the average HONO column concentration from 10 to 240 m) and HONO measured from the ground level to 10 m above the ground level (AGL). Column values were calculated for-(a) E3 and (b) C2.

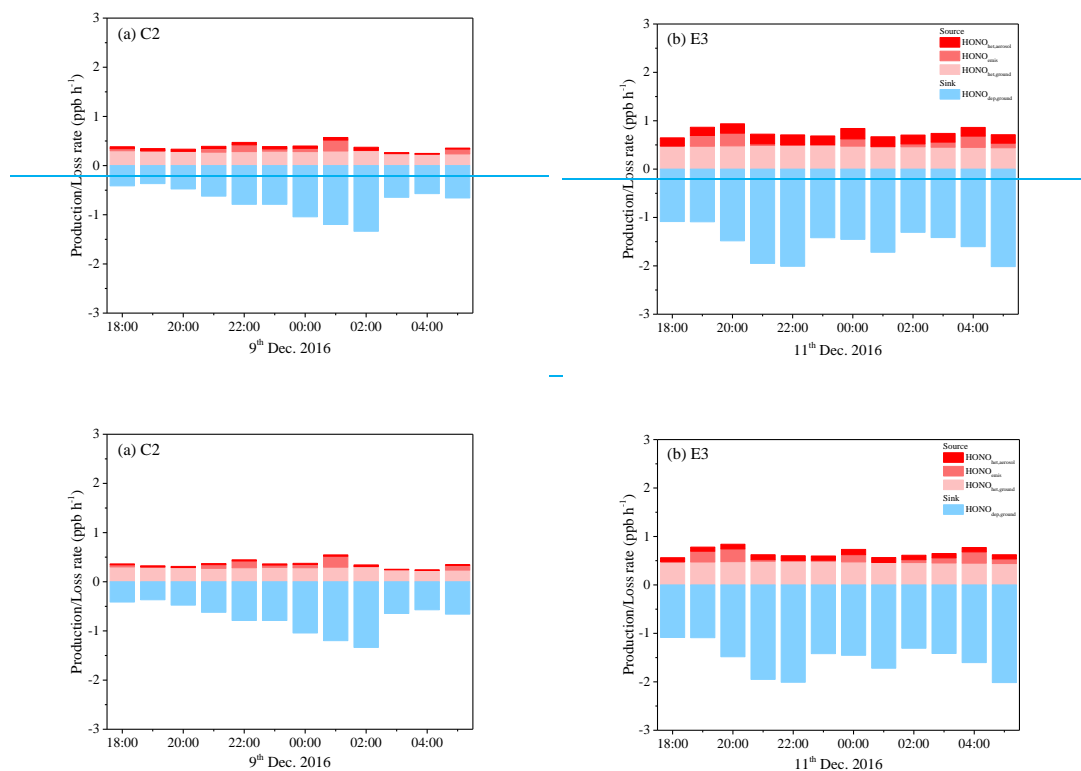


**Figure 11.** Separated contributions of production and loss terms (colored bars) of HONO on (a) the 9<sup>th</sup> (C2) and (b) 11<sup>th</sup> (E3) of December 2016. An upper limit uptake coefficient for NO<sub>2</sub> was adopted to calculate the HONO production rate on aerosol surface.